Methods for Predicting Flow-Induced Vibrations in Bellows Expansion Joints

by

Stephen L. Higgins

(Under the direction of R. Benjamin Davis)

Abstract

Bellows expansion joints are a specialty corrugated pipe fixture that serve critical purposes in aeronautics, space, defense and industrial applications. Their corrugated design makes bellows joints susceptible to a high-amplitude, flow-induced vibration phenomenon that can compromise the structural integrity of the joint. The current empirically-based method used by NASA to assess flow-induced vibration in bellows joints was developed in the early 1980s. This historical method is discussed here with a new nondimensional analysis that provides a simpler way to apply the model and examine its output. Presently, new bellows designs are beyond the empirical basis of this historical method, underscoring the need for more modern methods that are computationally efficient and physically insightful. To this end, a physics based, coupled oscillator model of bellows flow-induced vibration is developed. A comparison of the model output to experimental bellows response is presented and discussed.

Index words: Flow, Induced, Vibrations, Bellows, Expansion, Joint, Van der Pol, Oscillator

Methods for Predicting Flow-Induced Vibrations in Bellows Expansion Joints

by

Stephen L. Higgins

B.S., Georgia College and State University, 2011

A Thesis Submitted to the Graduate Faculty
of The University of Georgia in Partial Fulfillment
of the
Requirements for the Degree

Masters of Science

Athens, Georgia

2017

Methods for Predicting Flow-Induced Vibrations in Bellows Expansion Joints

by

Stephen L. Higgins

Major Professor: R. Benjamin Davis

Committee: Donald J. Leo
C. Brock Woodson

Electronic Version Approved:

Suzanne Barbour
Dean of the Graduate School
The University of Georgia
August 2017

Acknowledgements

I would like to express my sincere gratitude to my supervisor, Dr. Ben Davis, for providing me with this opportunity. Without his mentorship and continued encouragement I could not have completed this thesis.

Financial support from NASA grant NNX15AF84G, under the direction of Dr. Curt Larsen with the NASA Engineering and Safety Center, is gratefully acknowledged.

I am thankful to Dr. Andy Brown and Don Harris, with the Structural and Dynamics Analysis Branch at NASA Marshall Space Flight Center, for their guidance and for being wonderful hosts.

I graciously recognize Dr. Don Leo and Dr. Brock Woodson for serving on my committee. I would also like to acknowledge Campbell Dixon who assisted me as an undergraduate researcher.

To my family and my friends, Michelle, Dimitri and Travis, I am ever so thankful for your love and support while undertaking this endeavor.

Finally, I am thankful to the University of Georgia and the College of Engineering for the opportunity, the knowledge gained and for being a wonderful home during this chapter of my life.

Contents

List of Tables

List of Figures

Nomenclature

Symbols

A	coupling force scaling parameter
a	convolute crown radius
B_1, B_2	empirical constants
C	damping coefficient
$C_1 - C_7$	empirical constants
C_D	drag coefficient
C_f^o	coefficient of fluid force without motion, Eq (4.10)
C_f	coefficient of fluid force with motion
D_b	bellows inside diameter, Eq. (2.2)
D_f	design factor, Eq. (2.2)
D_m	mean diameter
D_p	inner diameter of upstream pipe, Eq. (3.16)
E	Young's modulus
F	force, Eq. (4.9)
f	frequency
$\overline{f}$	nondimensional frequency, Eq. (3.7)
h	convolute height
k	convolute stiffness
K_a	overall stiffness, Eq. (3.6)
L	live length, Eq. (3.16)
l	characteristic length

M	mass
m^*	structure-to-fluid mass ratio
N_c	number of convolutes
N_p	number of plys
n	mode number
P_D	dynamic pressure, Eq. (3.14)
q	wake variable
R_m	mean radius, Eq. (2.3)
S	strain, Eq. (4.23)
St	Strouhal number
SG	Skop-Griffin number, Eq. (4.24)
t	convolute thickness
t_p	corrected ply thickness, Eq. (2.2)
U	freestream velocity
U_r	reduced freestream velocity
w	model depth, circumference
x	displacement
X	nondimensional displacement, Eq. (4.14)
α	inner convolute width
β	specific spring rate, Eq. (3.13)
ϵ	van der Pol parameter
ζ	viscous structural damping ratio
η	mode number parameter, Eq. (3.8)
λ	convolute pitch
μ	nondimensional mass, Eq. (4.25)
ρ	density
σ	stress, Eq. (3.10)

$\overline{\sigma}$	nondimensional stress, Eq. (3.17)
τ	nondimensional time, Eq. (4.14)
ω	natural frequency

Subscripts

D	drag
fl	fluid
s	structure
R	real
I	imaginary

Conventions

i	imaginary unit $\equiv \sqrt{-i}$
$(\dot{o}), (\ddot{o})$	first, second derivatives with respect to time

Abbreviations

CFD	computational fluid dynamics
DOF	degree-of-freedom
FEM	finite element method
FIV	flow-induced vibrations
FSI	fluid-structure interaction
NASA	National Aeronautics and Space Administration
SDOF	single degree-of-freedom
SwRI	Southwest Research Institute
TM	technical memorandum
VIV	vortex-induced vibrations

Chapter 1

Introduction and Motivation

Bellows expansion joints are corrugated pipe fittings that serve critical purposes in aeronautics, space, defense, and industrial applications. First developed at the end of the 19^{th} century, bellows joints are used to absorb thermal deformation and isolate vibration. They are also used as a substitute for expansion loops to save space and prevent head loss. For aerospace applications, bellows are commonly used in rocket propulsion systems as part of feed lines to allow for articulation and reduction of misalignment loads. They can be described as having a number of uniform convolutions, much like an accordion, that are commonly U-shaped as seen in Fig 1.1.

Bellows are well suited for low pressure applications as over-pressurization can cause plastic deformation. There are numerous configurations and types of bellows each having advantages and disadvantages, but the most popular have U-shaped convolutions and are typically constructed by hydroforming thin walled cylinders of stainless steel or Inconel alloy. Metal U-shaped bellows are the only type examined in this thesis; however, the methods presented may be applicable to other bellows types.

The qualities that make bellows joints useful also make them susceptible to high-amplitude flow-induced vibrations (FIV). FIV is a phenomenon in which fluid flow interacting with elastic bodies induces motion. The response to this coupling of fluid and structural systems can cause fatigue failure. The phenomenon can be found across a wide range of engineering structures in applications such as power generation and transmission, aerospace, naval and civil engineering. In the case of bellows joints, as internal fluid flow passes over the cavities

Figure 1.1: Examples of single and double type bellows expansion joints (photograph by Peter Sonnabend, distributed under a CC-BY-SA 3.0 license)

formed by the convolutes, an oscillating shear layer develops across these gaps and impinges on adjacent, downstream convolutes. When the frequency of this oscillating shear layer matches a natural structural frequency of the bellows, large amplitude responses can occur. This is particularly challenging in the aerospace industry where the drive for lightweight components increases susceptibility to FIV.

There have been several bellows failures due to FIV. During the late 1960s and early 1970s, fuel subassemblies for the Japanese JOYO experimental fast breeder reactor were tested [1]. During testing there were a number of bellows, serving as components of sodium valves, that failed due to FIV, with one case resulting in a sodium leak. Numerous bellows failures occurred as part of the Joint European Torus fusion energy research project in the

1980s and early 1990s. Bellows leaks were the most significant item causing operational stoppages and delays [2].

Tragically, bellows fatigue was potentially responsible for an explosion at a chemical plant near Flixborough, England in 1974. The blast claimed 28 lives, seriously injured 36 others and completely destroyed the facility. Discounted by the original inquiry, more recent investigations suggest that an initial bellows failure, likely caused by FIV, released 10-15 tons of cyclohexane forming a vapor cloud that detonated with a force equivalent to 280 tons of TNT [3].

The bellows FIV phenomenon was first encountered by NASA during the second flight of the Saturn V rocket—the Apollo 6 mission—in which three J-2 engines malfunctioned. Bellows components of the LH_2 propellant lines failed due to fatigue caused by FIV on the S-II engine No. 2 and on the single S-IVB engine. The S-II No. 3 engine failed after receiving the shut down command intended for the ailing No. 2 engine due to crossed control wires [4]. The S-II stage was designed to compensate for the loss of a single engine, but the loss of both the No. 2 and 3 engines caused the spacecraft to achieve a less than nominal trajectory. Despite the failures, most of the missions parameters were achieved and the mission was considered a success.

The bellows failures during the Apollo 6 mission instigated a program of research that lasted into the early 1980s, in which NASA and its affiliate institutions studied the bellows FIV phenomenon. This research culminated in the 1983 NASA technical memorandum, TM-82556, which details a semi-empirical method for predicting fluid-loaded axial natural frequencies and flow-induced stresses in bellows joints of certain configurations [5]. This method is still in use by NASA and its contractors. Chapter 3 of this thesis presents this historical method along with a new nondimensional analysis that provides a simpler way to apply the model and examine its outputs.

Outside of NASA, bellows researchers in the 1960s developed approximate solutions for predicting structural frequencies and stresses as there is not a direct solution of the shell equa-

tions for a bellows' toroidal shape [6]. Anderson [7] developed design charts and equations for simplified calculations of bellows stresses; compensating for inaccuracies in the approximate solution with correction factors. His research forms the foundation of the guidelines set by the Standards of the Expansion Joint Manufacturers Association (EJMA) [8] for designing bellows joints. Numerical analysis has also been used to model bellows stresses using finite element and finite difference methods; however, to date, little research using computational fluid dynamics (CFD) techniques to model bellows internal flow or FIV characteristics has been published.

Presently, new bellows designs are beyond the empirical basis of the historical method, underscoring the need for more modern methods that are computationally efficient and physically insightful. To date, there does not exist a physics-based method of predicting this complex bellows fluid-structure interaction (FSI) phenomenon. The goal of this thesis is to develop an approach to predict bellows FIV that captures the salient physics of the phenomenon while dramatically reducing computational expense. To accomplish this, an FSI model that couples a discrete mechanical model of the bellows to a representation of the fluid wake expressed in terms of van der Pol oscillators is proposed in Chapter 4. This method reduces the computational expense of the problem by several orders of magnitude, requiring minutes compared to the weeks or months required for high-fidelity FSI simulations. Additionally, this model can be exercised across a large design space to better understand the physical parameters that strongly influence bellows FIV. This understanding will allow designers to select bellows joint configurations that minimize FIV potential. It will also enable the design of bellows joints to be more robust in the face of FIV.

Chapter 2

Background

While the earliest publication discussing bellows expansion joints was in 1946 [9], it was not until the 1960s and 1970s, with the rapid advance of power generation and aerospace technologies, that bellows research gained significant momentum. Much of this early research emanated from the United States Air Force [10] and NASA with their affiliate institutions [11–16]. NASA's research culminated in the 1983 technical report TM-82556 [5]. Since then, institutions worldwide have continued to provide new insights and methods of modeling the behavior of bellows joints. There are several key aspects of bellows systems that researchers have studied to develop more accurate prediction models, namely, bellows stiffness, axial and lateral vibrations, fluid-added mass, flow-induced vibrations, stress and fatigue.

2.1 Stiffness

The stiffness of bellows joints has been particularly challenging to model due to their unique geometry. TM-82556 [5] defines the bellows stiffness of one-half of a convolution as $k = 2N_cK_a$ and the overall stiffness as

$$K_a = \frac{D_m E t^3 N_p}{N_c h^3}, \tag{2.1}$$

where D_m is the bellows mean diameter, E is Young's modulus, N_p is the number of plys, N_c is the number of convolutes, t is ply thickness, and h is convolute height. See Fig. 2.1 for a

diagram of a bellows convolute with nomenclature. The authors advise that the user employ experimentally determined stiffness values if possible as the results were only approximate to experimental values.

Another method for calculating stiffness is included in the EJMA standards [8]. For one convolution the axial spring rate is represented as

$$k = 1.7\frac{D_m E t_p^3 N_c}{h^3 D_f}, \tag{2.2}$$

where $t_p = t\sqrt{D_b/D_m}$ is the corrected ply thickness to account for thinning caused during the forming process and D_b is the bellows inside diameter. The design factor D_f relates U-shaped convolution segment behavior to a simple strip beam and is determined using a design chart found in the EJMA standards [8].

Jakubauskas [17] was able to calculate the lateral stiffness of a bellows using the relation

$$EI_{eq} = \frac{1}{4}k\lambda R_m^2, \tag{2.3}$$

where I_{eq} is the equivalent second moment of area, k is the axial stiffness for one half of a convolution, λ is the convolute pitch, and R_m is the bellows mean radius. The accuracy of Eq. (2.3) is dependent on the accuracy of the provided k, which can be found by using the previously mentioned methods, experimentally or with finite element methods (FEM). For axial stiffness, Jakubauskas [17] also found that the half convolutions at the fixed ends of a bellows exhibited an increased stiffness due to their restrained condition. All other half convolutions had approximately the same stiffness.

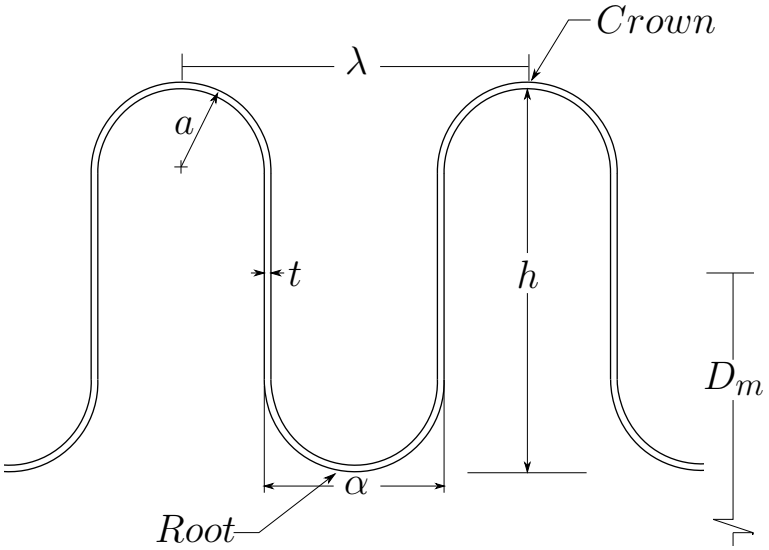

Figure 2.1: Convolute diagram with bellows nomenclature.

2.2 Axial Vibrations

Axial—also referred to as accordion or longitudinal—vibration is characterized by a sinusoidal displacement of the convolutes along the center axis of the bellows. Daniels [11] first discussed predicting axial modes for welded bellows and suggested using elastic, homogeneous bar formulas to calculate the axial natural frequencies and mode shapes. He verified his methods experimentally by mounting fluid filled bellows on a shaker table. Daniels' method of predicting axial natural frequencies was found to be accurate by Trainer, *et al.* [10] for both welded and formed type bellows. Lytle [18] modeled the bellows as a porous elastic cylinder and used a modified wave equation to calculate critical frequencies. His theoretical results compared within 9% difference to experiment; however, Lytle did not detail his experimental methods.

Morishita, *et al.* [19], modeled bellows by approximating them as fixed-fixed uniform rods. A seismic table was used to test a standard bellows restrained at both ends and with a flow sleeve. Tests were conducted with and without the bellows filled with water. Experiments compared within 20% to the predictions from the uniform rod model and from FEM analysis

for the first mode. Accuracy was better for the second and third modes with approximately 10% and 2% differences respectively.

Methods to determine axial natural frequencies of U-shaped bellows having different end conditions (fixed-fixed, fixed-free and fixed-free with a weight at one end) were developed by Li, *et al.* [20], by modeling the bellows as a pipe. Axial natural frequency results from experiments performed using tap testing were in good agreement with the model, having average percent differences within 6% for air and 9% for water. Radhakrishna and Rao [21] extended Li's work by developing a method for calculating axial vibrations for bellows with elastically restrained end conditions.

Jakubauskas and Weaver [22] modeled the bellows and the fluid region using axisymmetric shell and triangular finite elements, respectively. They verified the model using tap testing on a bellows with restrained end conditions, finding good agreement with just a 2% difference between theoretical and experimental natural frequencies in air and a corresponding 7% difference when filled with water. They also compared Gerlach's method [12] for predicting axial natural frequencies and concluded that its prediction was less accurate than their model for higher frequencies; however, the presented data show only a slight improvement of about 1% between the two methods for water filled bellows and 7% in air. A similar comparison was made with the axial frequency prediction method distributed by the EJMA [8]. It was found to be less accurate at higher modes with about a 6% difference for fluid-filled bellows and 11% difference in air.

2.3 Lateral Vibrations

Lateral—also referred to as transverse or bending—vibration in bellows has been studied in parallel with axial vibration. Daniels [11] used the same simple, elastic, homogeneous bar formula to model lateral modes while assuming the bellows to be a thin cylinder. While Daniels claimed the agreement between the predicted and experimental lateral frequencies for welded bellows to be fair, his data show differences averaging around 22%. Furthermore,

Trainer, *et al.* [10] observed that Daniels' methods did not accurately predict lateral frequencies for either welded or formed bellows. Li, *et al.* [20] also considered lateral modes of vibration using their same technique used for the axial case. They found that the lateral frequency predictions approached the experimental values, but were not as accurate as the predictions for the axial case, having about an 8% difference when filled with air and a 16% difference when filled with water.

Morishita, *et al.* [19] modeled lateral vibrations using Timoshenko beam theory. Timoshenko beam theory is an extension of Euler-Bernoulli beam theory that considers shear deformation and rotational inertia. It is useful for modeling short beams as it allows rotation between the cross section and the bending line, effectively decreasing the beam stiffness and changing the natural frequency. To validate the model, Morishita, *et al.* [19] subjected a standard bellows and a set of two bellows mounted in a segment of pipe to lateral excitation using a seismic table and found the first five natural frequencies. The results of the model compared favorably with the experiment and with an FEM analysis, with one notable exception. A bellows with a flow sleeve, i.e. a segment of pipe that extends into the bellows and shields the convolutes from direct flow, incurred significant error due to the fluid-structure interaction effect between the convolutions and sleeve. They determined that this effect could be accounted for with a virtual added mass concept that models the bellows as two coaxial cylinders [19]. They also compared the lateral modes of a standard bellows experiment to the EJMA [8] method and found that it drastically over-predicted the lateral natural frequencies. They attributed this to the EJMA method neglecting to account for rotary inertia.

Transverse vibrations were the subject of a doctoral thesis and reports by Jakubauskas [17] and Jakubauskas and Weaver [23, 24]. Their model was based on Timoshenko beam theory and included considerations for fluid-added mass, convolute distortion and rotary inertia. An exact solution and an approximate Rayleigh quotient formula were developed. Experimental results, found using tap testing on both single [23] and double [24] bellows

configurations, were compared with the model, and a method provided by the EJMA [8]. The model agreed within 5% of the experimental results for both air and water filled bellows, but the EJMA method drastically diverged from the experiment with increasing mode number due to neglecting rotational inertia and convolute distortion effects. When neglecting the effect of added mass due to convolute distortion in the model, a 140% difference was incurred. This difference increased to 240% when rotary inertia was also excluded. Jakubauskas and Weaver also found that the effect of shear deformation and the Coriolis force to be negligible for lateral modes. A vibrating pipe will have a Coriolis force component as the fluid velocity flows relative to the pipe while the pipe has some non-zero circumferential component to its motion. This effect was found to only alter the lateral natural frequencies by 0.5%. Broman, *et al.* [25] also modeled lateral bellows modes using his method discussed in Section 2.2. Comparison with the calculated and experimental results from Jakubauskas and Weaver [23] yielded an improved prediction of lateral frequencies of a few percent at higher modes.

Euler-Bernoulli beam theory with considerations for fluid-added mass and rotary inertia was used by Radhakrishna and Rao [26, 27] to model transverse vibrations for a rotationally restrained double bellows. In a separate study, they used Timoshenko beam theory with an approximated Rayleigh Quotient method to investigate lateral vibrations of multi-ply bellows with elastically restrained ends [28]. While there was no comparison with experiment, it was found that the approximated solution varied from the exact solution by as much as 33% for the first mode, suggesting that the Rayleigh Quotient method is insufficient for predicting natural frequencies of multi-ply bellows.

Jakubauskas and colleagues [17, 23] and Watanabe, *et al.* [29] have also found that increasing the internal pressure of bellows has the effect of significantly reducing the lateral frequency up to the point of buckling failure. Jakubauskas observed a lowering of the fundamental frequencies by about 7% when pressurized to 200 kPa, but the effect diminishes with increasing mode number. Watanabe, *et al.* [29] also found that lateral parametric reso-

nances occur in bellows subjected to internal periodic fluid pressure excitation. Parametric resonances are caused by varying a system parameter, in this case internal pressure, with time, and are twice the natural frequency. The effect was modeled and compared with the results from an experiment using a bellows with fixed ends, filled with oil, and an oscillating piston generating internal periodic pressure. The results are said to be in good agreement with experiment although they are presented in a graphic and not quantitative form.

2.4 Other Vibration Modes

In addition to axial and lateral modes, researchers have identified other vibration modes of bellows. Daniels [11] identified a"liquid mode" for welded bellows that he described as a motion of the bellows ends relative to each other that occurs when an excess amount of liquid in the convolutes is pumped in or out, effectively decreasing or increasing the liquid column and displacing the bellows end. It should be noted though that in Daniels' tests it appears that one end of the test bellows is free to move. No other researcher has documented this phenomenon and would seem unlikely to occur in most applications as bellows ends are usually restrained in some manner. The convolute bending mode is described by Gerlach, *et al.* [5] as a bending of the convolute walls and was only observed for high velocity gaseous flows with radial acoustic resonance. Torsional modes were modeled based on uniform rod theory by Broman, *et al.* [25]. He found that torsion natural frequencies were more than an order of magnitude higher than axial and lateral natural frequencies.

2.5 Fluid-Added Mass

As a body in fluid accelerates, some volume of the surrounding fluid is entrained. The entrained fluid effectively increases the inertia of the system. This phenomenon is referred to as fluid-added mass. This is critical to consider as the additional mass will affect the system's natural frequencies. In bellows joints, determination of the fluid-added mass is complicated by the convolute geometry and motion. The simplest method to account for

fluid-added mass is used by the EJMA [8], which considers only the mass of fluid contained between rigid convolutes. Gerlach's [12] methods included a fluid-added mass term with two components: the mass of the fluid trapped between the rigid convolutes and the varying mass as the convolutes are compressed and expanded. NASA TM-82556 [5] modified Gerlach's method to the one that is currently used by NASA. This approach is presented in Chapter 3.

Jakubauskas [30] established that the EJMA method was capable of accurately predicting the first few axial natural frequencies, but the error increased with increasing mode number. He modified the EJMA's method by including considerations for fluid-added mass due to convolution distortion and accounting for return flow back into the central area of the bellows cross section. With these modifications Jakubauskas was able to decrease the error in predicting axial natural frequencies for the first four modes to within a 2% difference relative to experiment; a drastic improvement over the prediction of a maximum 16.8% difference found using the original EJMA method.

In Jakubauskas and Weaver [31], a finite element analysis was performed to construct a distortion component for fluid-added mass when concerned with lateral vibration modes. They found that neglecting the effects of this distortion component on the fluid-added mass would result in an overestimation of the true bellows transverse natural frequencies. Desai and Thornhill [32] calculate fluid-added mass based on the longitudinal position of the convolutes in their numerical model (which is discussed further in Section 2.6.1).

2.6 Flow-Induced Vibrations

In general, modeling FIV can be challenging as the underlying excitation mechanisms can vary greatly. Several researchers have tried to generally classify FIV phenomena to better compare it across disciplines. Weaver [33] classified the excitation mechanisms into three groups based on the source of vibration: forced vibrations, self-controlled vibrations and self-excited vibrations. Forced vibrations are said to be induced by turbulent flow, are random

in nature, and the structure has a negligible effect on the fluid. For self-controlled vibrations, the fluid forcing has a periodic component and can induce large amplitude structural vibration if the fluid frequency is near a natural frequency of the structure. The amplitude of vibration will increase until the motion of the structure begins to control the frequency and magnitude of the fluid forces. The fluid velocity range over which this occurs is referred to as the lock-in region. Elastically restrained cylinders in flow, risers used on offshore oil platforms, and heat exchanger tube bundles are examples of systems that can experience self-controlled vibration. Self-excited vibrations also involve a periodic fluid force amplifying the structural motion, but the periodic force is originally created by motion of the structure. If a structural motion does not exist, the periodic fluid force will not occur. Aeroelastic flutter in wings and transmission line gallop are a couple of examples.

Naudascher and Rockwell [34] use a similar approach to distinguish between the excitation mechanisms, but elaborate on self-controlled vibrations or, as they call it, instability-induced excitation, by defining three types of instability controls: fluid-dynamic, fluid-elastic and fluid resonant. For the fluid-dynamic case the excitation force is only a function of the flow conditions. The excitation force of the fluid-elastic case is dependent on a coupling of the fluid force and an oscillating structure where as the fluid-resonant case depends on a coupling of the fluid force and a fluid oscillation. The latter is very important in compressible flows. The examples listed previously for self-excited vibrations are fluid-elastic systems. The Helmholtz resonator is a common example of the fluid-resonant case. The type of excitation mechanism at work in bellows FIV is a fluid-elastic instability-induced excitation (self-controlled in Weaver's parlance). For more information on FIV research and methods, the texts by Blevins [35] and Nakamura, *et al.* [36] are recommend in addition to those previously cited.

2.6.1 Bellows Flow-Induced Vibrations

The earliest researchers of FIV in bellows joints was C.R. Gerlach and his associates [12–14, 37,38]. They first theorized and concluded after experimentation that the excitation mechanism for FIV in bellows joints was caused by the frequency of fluid vortices shedding off of the bellows inner convolute tips matching a natural frequency of the bellows [12]. This behavior is akin to the classical case of vortex-induced vibration (VIV) of an elastically restrained cylinder subject to fluid flow. Gerlach found that the Strouhal number, a dimensionless number used to describe oscillating flow, can be used to predict the conditions at which maximum bellows excitation occurs. The Strouhal number is defined as $St = f_{fl}l/U$ where f_{fl} is the fluid frequency, l is the characteristic length and U is the flow velocity. Using the convolute root diameter, α, as the characteristic length, he found a Strouhal number range of $St \approx 0.1 - 0.3$ provided a good prediction of the vortex shedding frequencies that excite bellows structural response. VIV of an elastically restrained circular cylinder has approximately the same characteristic Strouhal number, leading Gerlach to believe in the vortex shedding hypothesis.

Gerlach developed a method for calculating the axial natural frequencies by modeling the bellows as a N-degree-of-freedom spring-mass mechanical system, where the springs and masses are in series and N represents one less than two times the number of convolutes. In 1972, Bass and Holster [15] expanded on Gerlach's work by conducting bellows testing with internal cryogenic flow. They found that heat transfer causes local boiling in the convolutes, which suppresses vortex formation and dampens the system. Bass and Holster also found that the build up of frost on the outside of the bellows with cryogenic flow had negligible effect on the amplitude of FIV; however, light and heavy ice formations could potentially reduce or completely eliminate vibrations. Two reports, Johnson, *et al.* [16], conducted at the Southwest Research Institute (SwRI) in 1979, and NASA TM-82556 [5], conducted at Marshall Space Flight Center in 1983 and led by Gerlach, used Gerlach's earlier frequency prediction methods and carried out extensive testing on a large variety of bellows. The

resulting model is capable of predicting axial vibration frequencies and flow-induced stresses, and is still in use today by NASA. A 1986 report by Desai and Thornhill [32], prepared under a NASA contract, adopted a different approach to predicting bellows FIV. They determined that the TM-82556 method of predicting stresses and natural frequencies was too conservative and were concerned about its reliance on empirically based functions. The researchers developed a lumped parameter vibration model that coupled convolute motion in the axial and lateral directions. The model required numerical methods to solve for time-dependent displacement, from which the frequency could be calculated using Fourier analysis. While unique, the model could only be applied to bellows having five or less convolutes due to the cycles until failure prediction decreasing unrealistically. Furthermore, there was no comparison between the predicted natural frequencies and experiment.

In contrast to vortex shedding being the excitation mechanism, the other theorized possibility is that bellows FIV is caused by impinging free shear layer instabilities over the periodic cavities formed by the convolutions. Rockwell and Naudascher [39] first suggested bellows FIV as a cavity driven oscillation in 1978 and compared it to similarly proportioned rectangular cavities which generally have characteristic Strouhal numbers of $St \approx 0.5$. They explained the difference between Gerlach's Strouhal number and their own by suggesting that the rounded corners of a bellows cavity have the effect of lowering the oscillation frequency. However, it seems improbable that this would explain a nearly twofold difference in St. What Rockwell and Naudascher failed to mention or realize was that Gerlach used the convolute root diameter, α, as the characteristic length while they used the length of the cavity opening in the stream-wise direction. In the case of a bellows this cavity length would be the convolute pitch, λ, shown in Fig. 2.1.

Weaver and Ainsworth [40], who experimentally investigated the FIV failure of a double bellows used in the Joint European Torus fusion energy project, supported the concept of free shear layer instability as the excitation mechanism. They found that the Strouhal number, based on the convolution pitch and corresponding to the peak vibration amplitude in each

mode, was consistent with that of free shear layer instability over a deep cavity, finding a Strouhal number of $St = 0.45$ for the bellows tested. Gidi and Weaver [41,42] built and tested a two dimensional convolute model in a flow loop, described in more detail in Chapter 4, to visually examine the phenomenon and arrived at the same conclusion. Watanabe [29] sought to further evaluate the flow pattern around bellows and evaluate the excitation mechanism. He created a similar two-dimensional model except that the convolutions were formed by placing masses on the end of plate springs and were not coupled together. He concluded from flow visualization studies that shear layer instability is the excitation mechanism, but also suggested that a fluid elastic feedback system caused by a periodic vortex street synchronizing with the moving convolutes has a significant role on the instability mechanism as well.

A survey of the bellows mentioned in the literature indicates that, for a typical bellows, λ ranges between 1.5α and 2α with an average around 1.7α. One can compare the open cavity flow theory constructed by Rockwell [43] with experimental bellows data to help determine a representative St range for bellows. For Rockwell's theory, he compared St with the length of the open cavity divided by the cavity height. In bellows these dimensions correspond to convolute pitch, λ and convolute height, h. The available bellows experimental data have a narrow St range of $0.42 - 0.50$ for multiple modes with the exception of the Bass and Holster [15] data, which is confounded by the effects of an upstream elbow. This is in contrast to Gerlach's [14] wider range of $St \approx 0.1 - 0.3$. The bellows data fit very well with the theory for the first fluid mode response for deep, rectangular cavity flow despite the geometric differences.

Jakubauskas [17] and Jakubauskas and Weaver [23,24] also experimentally studied lateral FIV of single and double bellows. They found that internal flow in bellows can excite its lateral modes and that the static method mentioned in Section 2.3 is capable of accurately predicting the flow-exited frequencies. A Strouhal number of $St = 0.45$ was again found to be appropriate.

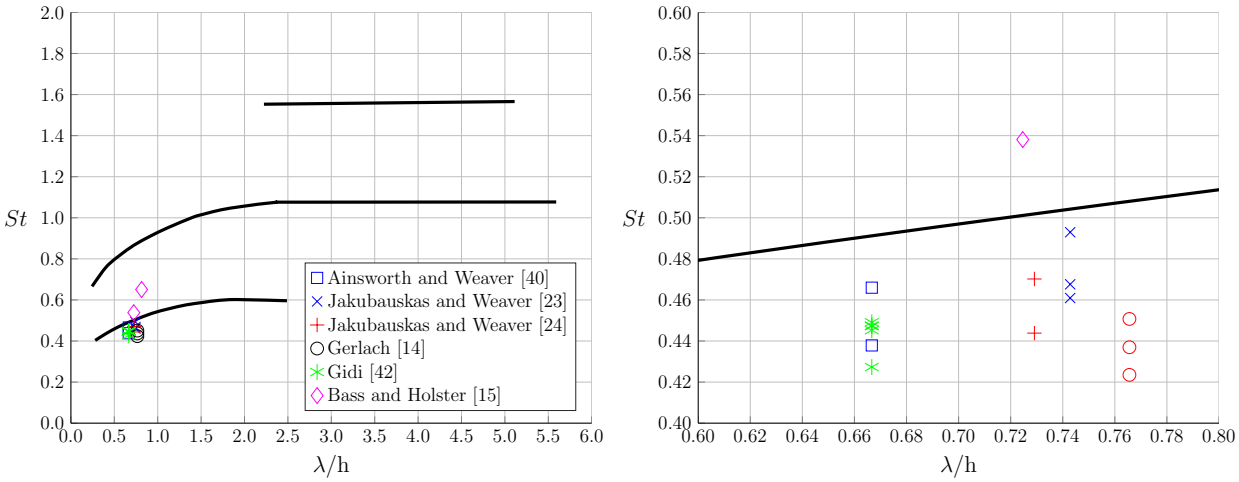

Figure 2.2: Experimental bellows data overlaid on Rockwell's [43] Strouhal number vs. pitch/height ratio chart, (a), with detailed area, (b)

2.6.2 Flow-Induced Acoustic Resonance

Baylac, *et al.* [44] studied the acoustic behavior of bellows joints with flow sleeves used in a piping system carrying pressurized CO_2 for a nuclear reactor. It was found that the cavity between the flow sleeve and convolutions could potentially act as an acoustic resonator and induce stress on the bellows. By modeling a two-dimensional resonator, they were able to predict the first six natural frequencies with less than ten percent error. Popescu and his colleagues [45–47] studied flow-induced acoustic resonance in corrugated pipes with applications to riser pipes used on drill platforms. They modeled the acoustic response with a one-dimensional, transient model that couples the wave equation and a van der Pol oscillator equation to simulate the flow-induced oscillations over convolute cavities. The model's frequency predictions agreed within 1.3% of the experimental frequencies and is able to predict lock-in velocity and onset fluid velocity.

2.6.3 Effect of Upstream Flow Conditions

In typical bellows installations it is not uncommon for the operational flow conditions to be nonuniform due to an upstream elbow or bend in the piping system. Johnson, *et al.* [16]

and TM-82556 [5] first studied the effect of an upstream elbow on bellows joints. It was found that, in the presence of an upstream elbow, the mean flow velocity required to excite a given mode is shifted downward and the amplitude of flow-induced stress (FIS) is increased. TM-82556 attempts to account for the effect of an elbow on FIS, but does not make any considerations for shifting the velocity.

Similarly, Weaver and Ainsworth [40] found that nonuniform upstream velocities resulted in the reduction of the mean velocity necessary to excite a resonant response as the bellows could be excited by sufficiently high flow velocities over just a portion of the bellows circumference. They concluded that elbows and sudden transitions immediately upstream of the bellows should be avoided to maintain uniform flow. Jakubauskas [23] found that the presence of an 90^o elbow immediately upstream can reduce the mean flow velocity required to excite a resonance response by an average of 29% and resulted in an increase in average Strouhal number to $St = 0.574$.

2.7 Bellows Stress and Fatigue

The determination of the fatigue life of bellows joints due to FIV is paramount. The ability to accurately quantify the serviceability of these critical components is necessary to ensure reliable operation. However, predicting the operational life span of bellows joints is very complex due to the variety of bellows designs and associated flow environments. An excellent review of bellows deflection and stress models prior to 1986 was written by Becht [48] in which he presents a detailed summary of theoretical and analytical models. General elastic shell theroy modified for axisymmetric shells is one example. Numerical methods used include finite-element and finite-difference methods and numerical integration, with the latter two being used to solve shell equations. Analytical methods used for predicting both axial and bending stress include beam and cylinder approximations, shell theory, elastic numerical analysis and nonlinear numerical analysis.

Following this review, Osweiller [49] develped a finite element program based on linear

elastic theory for predicting stresses due to axial displacement and internal pressure. Comparison with the EJMA standards yielded good results. A "linear bellows element" is proposed by Mackenzie and Boyle [50] for use in an finite element program. Li, *et al.* [51] also used a finite element model for stress and fatigue prediction and determined from testing that fatigue cracks usually originate from the positions of maximum strain located at the roots. Schonberg, *et al.* [52] carried out testing on bellows with U-shaped convolutes and found that common commercially available flat strain gauges were inadequate for measuring thin-walled, formed, metal bellows with small convolute radii. To calculate stress for axial modes Morishita, *et al.* [19] simply used the model provided by the EJMA [8], but combined this model with other considerations to develop a stress model for transverse modes. This model, however, has not been confirmed experimentally. Becht [53] focuses on trying to understand strain effects in bellows to reduce the amount of fatigue tests required for bellows design. The effects that corrosive media have on the fatigue of bellows was the concern of Zhu, *et al.* [54], which found that corrosive media can accelerate bellows crack initiation and propagation rates. Stelmar [55] complied a substantial amount of stress and fatigue data for bellows joints to compare with EJMA and ASME prediction methods and presents an empirically-based S-N curve.

Gerlach first introduced his "stress indicator" approach in 1972 [14]. After comparison with extensive testing this method did not accurately predict the behavior of bellows failure. It neglected to recognize the effect of the mode number. The "$C_F Q$" approach, proposed in Johnson, *et al.* [16], was a modification of the stress indicator method in an attempt collapse the experimental data along a single relationship by including considerations for the effect of mode number. This method was also found to be inadequate as it failed to account for the non-linear damping behavior of bellows. The final model deviated from the previous methodology and used empirical coefficients to fit the model to the experimental stress data. This method is currently still in use as part of NASA TM-82556 [5] presented in Chapter 3.

Chapter 3

Analysis of Historical NASA Method: TM-82556

NASA Technical Memorandum (TM)-82556 [5] is the culmination of almost two decades of research on bellows FIV by NASA and SwRI. Through extensive testing, a semi-empirical model was developed to predict bellows axial natural frequencies and flow-induced stresses. This method is still being used by NASA and its affiliate institutions; however, it is being applied to bellows configurations that are outside of its experimental basis. To better understand and evaluate the TM-82556 method, which can be something of a black box for users, it is presented here in a succinct format. Through a nondimensionalization of its key equations, its predictions are also compared to existing experimental data.

3.1 Axial Natural Frequencies of Bellows Joints

TM-82556 describes a bellows joint as a series of springs and masses, as shown in Fig. 3.1, where each root and crown is assigned as a mass for a total of $s = 2N_c - 1$ masses.

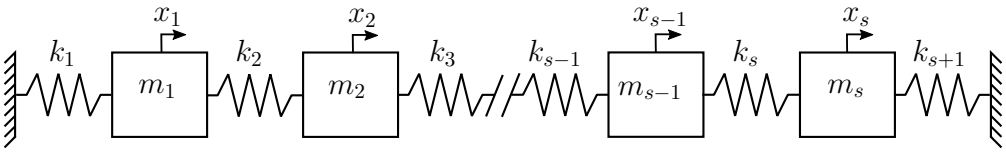

Figure 3.1: TM-82556's spring-mass representation of a bellows joint.

The formula for the axial natural frequencies of this bellows model is

$$f(n) = \frac{1}{\sqrt{2}\pi}\sqrt{\frac{k}{m_t}\left(1 + \cos\left(\frac{\pi(2N_c - n)}{2N_c}\right)\right)}, \tag{3.1}$$

where n is the axial mode number ranging from $1 \ldots 2N_c - 1$, N_c is the number of convolutes and the total mass, m_t, is equal to the sum of the structural mass, m_s, and the fluid-added mass, m_{fl}. The structural mass is defined by

$$m_s = \pi \rho_s D_m t N_p (\pi a + h - 2a), \tag{3.2}$$

where ρ_s is the structural mass density, D_m is the mean diameter of the bellows, N_p is the number of plys, t is the ply thickness, a is the mean convolute radius and h is the mean inside convolute height, (see Fig. 2.1). The fluid-added mass is given by

$$m_{fl} = B_1 m_{fl_1} + B_2 m_{fl_2} \left(\frac{n}{N_c} \right), \tag{3.3}$$

where B_1 and B_2 are empirical constants having values 1.0 and 0.68, respectively. The m_{fl_1} and m_{fl_2} terms are

$$m_{fl_1} = \frac{\pi \rho_{fl} D_m h (2a - t N_p)}{2}, \tag{3.4}$$

and

$$m_{fl_2} = \frac{\rho_{fl} D_m h^3}{\lambda - \alpha}, \tag{3.5}$$

where ρ_{fl} is the fluid mass density, λ is the convolute pitch and α is the convolute root width. Equation (3.4) is used to calculate the fluid-added mass contained within one-half of a convolute and Eq. (3.5) accounts for the fluid-added mass due to convolute distortion. The bellows stiffness of one-half of a convolution is defined as $k = 2N_c K_a$. The bellows spring rate, K_a, is given by

$$K_a = \frac{D_m E N_p t^3}{N_c h^3}, \tag{3.6}$$

where E is the Young's modulus.

3.2 Nondimensional Analysis of the Axial Natural Frequency Formula

A nondimensional version of the axial natural frequency formula, Eq. (3.1), is shown here. This expression allows the TM-82556 prediction of axial natural frequencies to be compared to experimental frequency data across a range of bellows designs. The nondimensional frequency function, $\overline{f}$, is given by

$$\overline{f} = \sqrt{\frac{m_t}{k}} f(n) = \frac{1}{\sqrt{2}\pi} \sqrt{1 + \cos\left(\pi \frac{2N_c - n}{2N_c}\right)}. \tag{3.7}$$

To compare axial natural frequency predictions across designs with varying N_c it is helpful to cast $\overline{f}$ in terms of a mode number parameter, that is itself a function of N_c. This mode number parameter, η, is defined as

$$\eta \equiv \frac{2N_c}{2N_c - n} \quad \text{for } n = 1, 2, \ldots, 2N_c - 1, \tag{3.8}$$

and increases linearly with increasing mode number. The nondimensional frequency expression in terms of η is now

$$\overline{f} = \frac{1}{\sqrt{2}\pi} \sqrt{1 + \cos\left(\frac{\pi}{\eta}\right)}. \tag{3.9}$$

The available experimental natural frequency data consider bellows joints of a variety of designs. Using Eq. (3.9), it is now possible to compare these experimentally determined natural frequencies to the TM-82556 prediction on the same plot shown in Fig. 3.2. Experimental data is compared from many sources—TM-82556, Gerlach [14], Ainsworth and Weaver [40], Jakubauskas and Weaver [22, 24], Morishita, *et al.* [19], Bass and Holster [15] and Li, *et al.* [20].

Examining the percent error between the data sets in Table 3.1, it is observed that the data collected by NASA [5] and Gerlach [14] have a good fit to the predicted frequency curve with the exception of three bellows [13]. These discrepancies may be because the pro-

vided geometry for these three bellows is slightly inaccurate causing an incorrect prediction using Eq. (3.6). It was noted by the authors that the reported geometric values were a representation and may not be completely accurate [13].

The Jakubauskas and Weaver [22], Morishita, *et al.* [19] and Li, *et al.* [56] data sets also compare favorably with the prediction. Of the remaining three data sets, Bass and Holster [15] is unique in that it involves cryogenic flow testing. Data for both water and liquid nitrogen flow tests are listed and both sets have significant percent error. The only potential flaw apparent in the experimental configuration is that their flow loop had the pump and an elbow placed immediately upstream of the joint; however, the frequency should not vary with an upstream elbow [24]. Another possibility for the high error is an incorrect prediction of the stiffness calculated using Eq. (3.6), as it was not provided in the report.

The last two data sets, Ainsworth and Weaver [40] and Jakubauskas and Weaver [24], used double bellows configurations. The Ainsworth and Weaver double bellows consisted of two, five convolute bellows separated by a section of pipe for a total of ten convolutes in the axial direction. The Jakubauskas and Weaver double bellows was made up of two, 13 convolute bellows for a total of 26 convolutes in the axial direction. The Jakubauskas and Weaver bellows shows excellent agreement with the prediction, but the Ainsworth and Weaver bellows has the highest percent error of all the data. This is thought to be caused by either geometric irregularities in the bellows or an over-estimated prediction by the TM-82556 method for calculating stiffness. The geometric irregularities imaged in the report show that the outer convolutes are not symmetric to the inner convolutes; additionally, the convolute roots protrude into the mean flow, unlike all other bellows examined. The Ainsworth and Weaver case is interesting as it shows that asymmetrical geometries could have a significant impact on bellows FIV characteristics. In Fig. 3.2, 85% of the data falls within 20% of the $\overline{f}$ prediction.

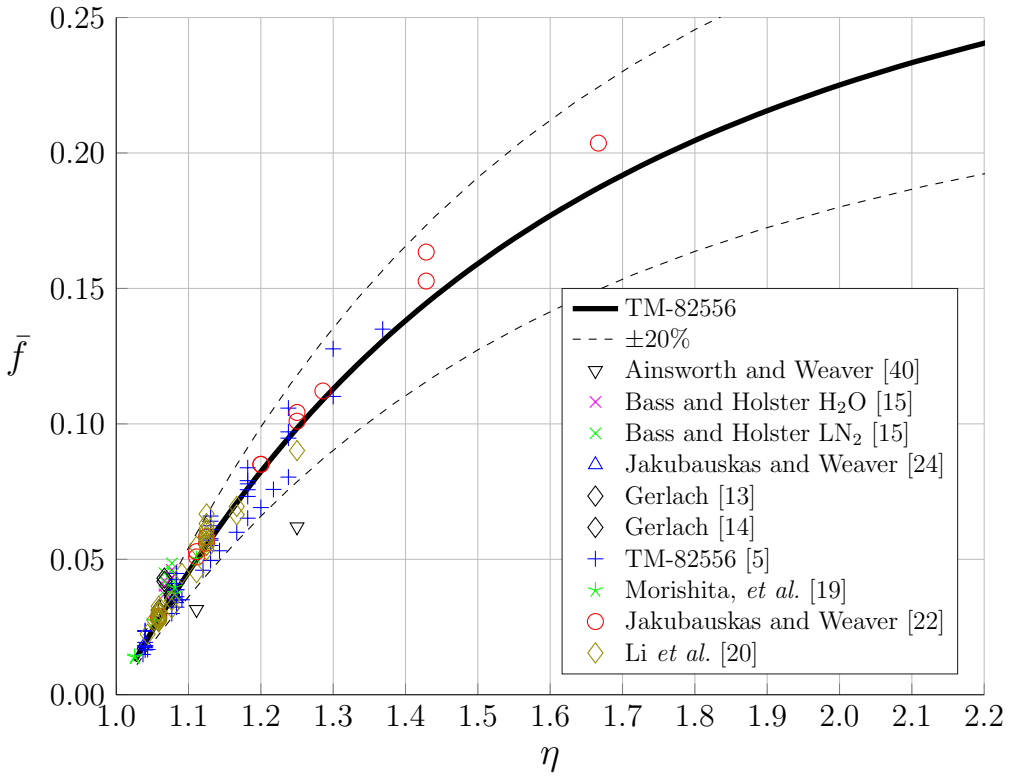

Figure 3.2: Prediction curve and experimental data in terms of nondimensional frequency $\overline{f}$ versus η (85% of the data lies within ±20% of $\overline{f}$)).

Table 3.1: Percent error between TM-82556 nondimensional frequency $\overline{f}$ prediction and experimental data.

Data Set	**Points**	**Max % Error**	**Abs. Mean % Error**
Ainsworth and Weaver [40]	2	37.0	37.0
Bass and Holster w/ H_2O [15]	6	-35.4	23.7
Bass and Holster w/ LN_2 [15]	6	-44.2	30.6
Jakubauskas and Weaver [24]	2	6.2	3.4
Gerlach [13]	3	-38.0	28.6
Gerlach [14]	3	-4.4	2.9
TM-82556 [5]	46	-24.5	9.4
Morishita, *et al.* [19]	7	-8.63	3.8
Jakubauskas and Weaver [22]	14	-13.1	4.9
Li, *et al.* [20]	32	-21.1	6.8
Total	121	-44.2	10.1

3.3 Stress Function

As bellows joints deform in the axial direction, the peak stress is located at the roots and crowns of the convolutes. Bellows operating in FIV conditions can experience cyclic fatigue with failures usually located at these peak stress locations. TM-82556 presents the formula for calculating this peak flow-induced stress as

$$\sigma = \frac{1}{U'}\left(\frac{C_1}{C_2 + U'^2} + \frac{C_3 \mid \sin(\pi U') \mid}{C_4 + U'^2} + C_5\right)\frac{C_P C_E C_R t E P_D}{\delta \beta N_p}. \tag{3.10}$$

The coefficient, C_P, is a damping modifier for multi-ply bellows defined by

$$C_P = \begin{cases} 1 & \text{if } N_p = 1, \\ \left(1 - \frac{C_6}{1+C_7(U'^2)}\frac{\alpha}{h}\right) & \text{if } N_p > 1. \end{cases} \tag{3.11}$$

This coefficient is needed to account for Coulomb friction damping occurring between the plys. The empirical constants $C_1 - C_7$ have values 0.130, 0.462, 1.000, 10.000, 0.060, 1.250 and 5.500, respectively. The C_R coefficient is expressed as

$$C_R = 1 + 0.1\left(\frac{400}{\beta}\right)^2, \tag{3.12}$$

where 400 is a reference spring rate and β is the specific spring rate of the bellows given by

$$\beta = \frac{K_a N_c}{D_m N_p}. \tag{3.13}$$

The dynamic pressure, P_D, is defined as

$$P_D = \frac{\rho_{fl} U^2}{2}, \tag{3.14}$$

where U is the fluid freestream velocity at mode n. This flow velocity can be calculated using $U = \alpha f(n)/St$, where St is the Strouhal number. TM-82556 defines a range of $St = 0.1 - 0.3$

with a critical $St = 0.2$. The U' variable is the result of dividing U by the critical velocity, U_c. The critical velocity is the velocity of the fluid freestream at which the bellows is excited at $n = N_c$. It is also useful to define U' in terms of a nondimensional frequency ratio, f', shown using the Strouhal number:

$$U' = \frac{U}{U_c} = \frac{\frac{\alpha f(n)}{St}}{\frac{\alpha f(N_c)}{St}} = \frac{f(n)}{f(N_c)} = f'. \tag{3.15}$$

The elbow factor, C_E, accounts for the effects of an elbow upstream of the bellows and is defined as

$$C_E = \begin{cases} 1 & \text{if absent,} \\ 1 + \frac{4.7}{2.0 + L/D_p} & \text{if present,} \end{cases} \tag{3.16}$$

where L is the length from termination of an upstream elbow to the first convolute of a bellows joint divided by the inner diameter of the pipe, D_p, just before the start of the joint.

3.4 Nondimensional Analysis of Stress Function

A nondimensional statement of the stress function, Eq. (3.10), was formulated and is denoted $\overline{\sigma}$. This new function allows for the comparison of stresses for bellows of varying geometries. The new formulation is expressed as

$$\overline{\sigma} = \frac{\delta \beta N_p}{C_E C_R t E P_{D_c}} \sigma = C_P U' \left(\frac{C_1}{C_2 + U'^2} + \frac{C_3 \mid \sin(\pi U') \mid}{C_4 + U'^2} + C_5 \right), \tag{3.17}$$

where

$$P_{D_c} = \frac{\rho_{fl} U_c^2}{2}, \tag{3.18}$$

is the result of multiplying P_D, Eq. (3.14), by $(U_c/U_c)^2$ and moving the resulting U'^2 to the right hand side.

This nondimensional stress formulation is not as straight forward as that for the non-dimensional frequency. When $N_p = 1$ the experimental data of one ply bellows can be compared to one predicted curve; however, due to the conditionality of Eq. (3.11), when $N_p > 1$ there exists the geometric ratio α/h. Because of this ratio, experimental data for multi-ply bellows can not collapse along a single curve. A reasonable range could be approximated based on minimum and maximum values of the α/h ratio (0.4 and 0.75) for typical bellows.

To compare experimental data with the predicted curves generated by the right-hand side of Eq. (3.17), the experimental peak stress, the U_c calculated by the model, and the bellows geometry and material properties must be entered into the left-hand side. The U' values of the data points in Fig. 3.3 are calculated by dividing the experimental velocity, U, at peak stress by the predicted U_c. Figure 3.3 contains the experimental data plotted with the predicted single and multi-ply curves. Experimental data were obtained from TM-82556 and Johnson, *et al.* [16] with stress values ranging between 1.9×10^8 Pa and 2.6×10^8 Pa and between 4.8×10^6 Pa and 6.2×10^7 Pa respectively. Examining Fig. 3.3 and Table 3.2, the single ply data from TM-82556 has an absolute mean percent error of 17.2% while the multi-ply data have good agreement with a absolute mean error of 7.1%.

Both the single and multi-ply data from Johnson, *et al.* [16] have significant error. One potential source of error that could account for the large difference between the two reports is stiffness. The stiffness values used for the TM-82556 data were experimentally found while Johnson, *et al.* [16] never discussed the origin of the provided stiffness values. TM-82556 showed that the true stiffness of bellows could vary significantly from the value provided by the manufacturer [5]. Using Eq. (3.6) to calculate the stiffness for the Johnson, *et al.* data does increase the accuracy. The single-ply data sees a moderate mean error reduction to 50.3% while the multi-ply data has a significant improvement with a new mean error of

15.3%.

An over-prediction of FIS was expected knowing that TM-82556's authors often cited conservatism throughout its development [5, 13, 16]. TM-82556 notes that the "predicted FIS values are always greater than actual values, hence, the model is conservative [5]." In fact, all of the experimental stress data presented from TM-82556 was over-predicted by the dimensional model and fit within 20% of its prediction. This conflicts with Fig. 3.3, which shows all of the single-ply and a few of the multi-py TM-82556 data points being under-predicted. This can be explained by the true critical velocity of the experiment deviating from the predicted U_c for $St = 0.2$. If the experiment's critical velocity was observed, substituted into Eq. (3.18), and used to calculate U' the result should match that of the dimensional model. Without this information, results can deviate in both $\overline{\sigma}$ and U'.

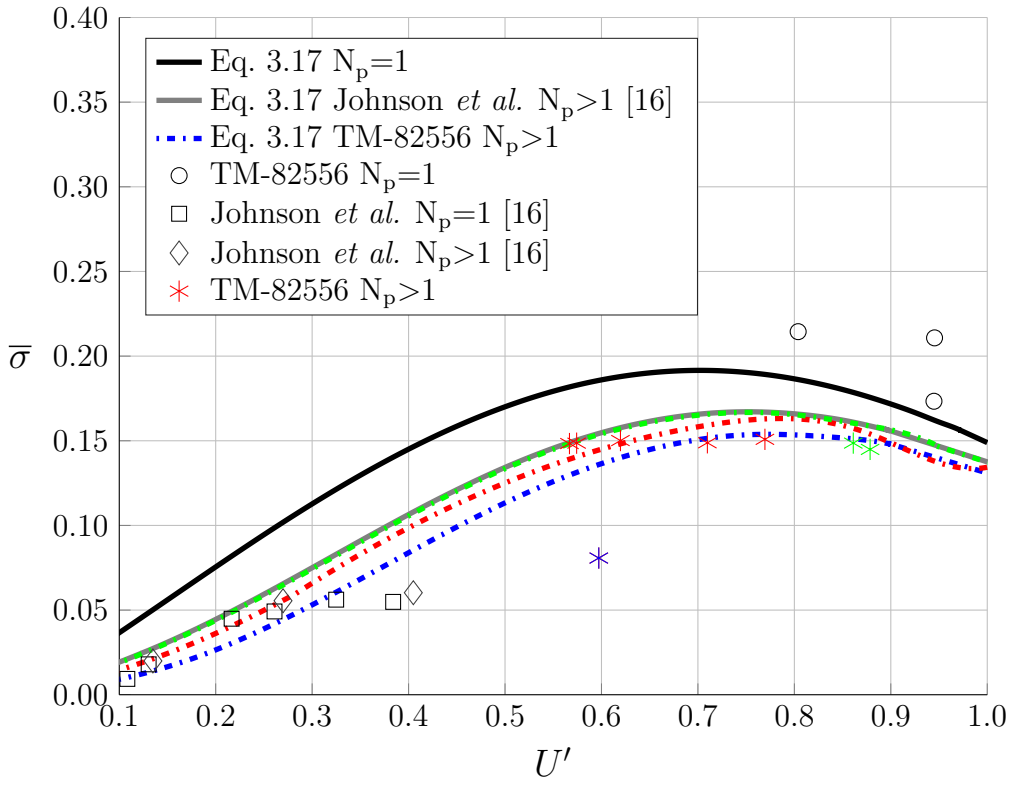

Figure 3.3: Comparison of predicted curves for nondimensional stress $\overline{\sigma}$ versus U' with experimental data.

Table 3.2: Comparison of predicted curves for nondimensional stress $\overline{\sigma}$ versus U' with experimental data.

Data Set	**Points**	**Max % Error**	**Abs. Mean % Error**
TM-82556 $N_p = 1$	3	-29.6	17.2
TM-82556 $N_p > 1$	8	40.6	10.52
Johnson, *et al.* [16] $N_p = 1$	6	76.6	58.2
Johnson, *et al.* [16] $N_p > 1$	3	44.2	28.9
Total	20	76.6	28.6

3.5 Discussion of Nondimensional Versions of TM-82556 Methods

Expressing the TM-82556 method in a nondimensional format offers a unique perspective on the model. As shown, the nondimensional formulation for the frequency equation allows comparison over a wide range of bellows configurations with a single prediction curve. It has also been shown to be accurate when compared with a large amount of experimental data from many sources. The nondimensional formulation for the flow-induced stress equation yields a single prediction curve for single ply bellows and a prediction range for multi-ply bellows. Even though the experimental data sets used for comparison are somewhat limited, TM-82556 appears to reasonably predict FIS.

Figures 3.2 and 3.3 along with Eqs. (3.7) and (3.17) can be used to predict frequency and flow-induced stress with only hand-calculations. The steps to find the frequency are:

1. Calculate η using Eq. (3.8) for the desired mode.

2. Find $\overline{f}$ by comparing the value for η with the predicted curve in Fig. 3.2 or by solving Eq. (3.9).

3. Frequency can then be found using:

$$f(n) = \sqrt{\frac{k}{m_t}}\overline{f} \tag{3.19}$$

where $k = 2N_cK_a$, with K_a being calculated using Eq. (3.6), and m_t is the sum of the structural mass, Eq. (3.2), and fluid mass, Eqs. (3.3)-(3.5).

To calculate flow-induced stress:

1. Use the above process and Eq. (3.19) to calculate $f' = f(n)/f(N_c)$ for the mode, n, of interest.

2. Compare f', which is equal to U', with the predicted single ply curve or approximate range for multi-ply curves on Fig. 3.3 to determine nondimensional stress $\overline{\sigma}$.

3. Dimensional stress is then calculated using $\overline{\sigma}$, geometric and material properties as inputs into:

$$\sigma = \frac{C_E C_R t E P_c}{\delta \beta N_p} \overline{\sigma} \tag{3.20}$$

TM-82556 includes consideration for the effect of an upstream elbow in the form of the elbow factor, Eq. (3.16), which modifies the FIS calculation. It does not, however, include considerations for adjusting the velocity range over which excitation occurs. It is thought that the downward shift in the velocity range due to an upstream elbow would translate to both U and U_c, leaving the ratio U' relatively unchanged for the nondimensional formulation. In practice, U' could potentially be calculated for a bellows without an elbow present and then be applied to the elbow case. This would provide an elbow corrected $\overline{\sigma}$ with the appropriate U' value. There was not enough information to determine U' in the TM-82556 results for the bellows tests with an upstream elbow to compare the data using the nondimensional method.

Chapter 4

A Coupled Oscillator Model of Flow-Induced Vibration in Bellows

Here bellows FIV is modeled using a series of considerations that are supported by prior work. First, it is assumed that vortex formation occurs in a bellows joint due to self-sustained oscillations of impinging shear layers [39, 57]. It then follows that the fluid oscillatory frequency depends on the convolute pitch, λ, not the convolute width, α [39, 40]. It is also presumed that convolute motion increases the vortex strength. Rockwell and Naudascher describe this as "movement-induced leading-edge vortices" in which the movement of a bellows convolute generates enhanced vortex formation in the shear layer [34].

Further, it is postulated that the model should exhibit a frequency lock-in phenomenon in which the fluid oscillatory frequency and the bellows structural frequency "lock" together across a potentially wide range of freestream velocities. In bellows, this phenomenon has been discussed by Gerlach and his colleagues [5, 12–14, 37] and the shape of response curves from experimental data are indicative of lock-in. Finally, it is presumed that at a certain point, the amplitude of the convolute motion will be detrimental to vortex strength. This will lead to convolute response amplitudes that are self-limited.

A model that exhibits the above features while remaining simple and computationally inexpensive is sought. The proposed modeling approach is inspired by a model of an elastically-restrained, single degree-of-freedom cylinder subject to uniform flow. The model couples the structural equation of motion of the cylinder to a van der Pol equation modeling the fluctuating lift associated with the vortex wake [58]. While the model is relatively simple, it captures the classical FSI phenomena associated with VIV; namely, self-limiting response amplitudes

and frequency lock-in. Here, this cylinder VIV model is adapted for use with bellows joints. Bellows response is calculated and compared to experimental responses available in literature. The model is also exercised across a wide range of bellows mass, damping, and fluid forcing conditions to observe the possible FIV amplitude and frequency lock-in behavior.

4.1 Van der Pol Oscillator in FSI Models

The use of a wake oscillator equation to model near wake dynamics in fluid-structure interaction systems was proposed and developed by Birkhoff and Zarantonello [59]. This was supported by experimental data gathered by Bishop and Hassan [60] while studying cylinder VIV in flow. They found that fluid oscillators exhibit non-linear, self-excited behaviors. Hartlen and Currie [61] were the first to couple the van der Pol oscillator with the cylinder motion via a linear dependence on the cylinder's velocity. While this model compared well with many features of the experimental results (e.g. the cylinder amplitude response when the shedding frequency was close to the structural natural frequency) Skop and Griffin [62] felt that the model was underdeveloped because the model parameters were not related to physical parameters of the system. They in turn developed a modified version of the Hartlen and Currie [61] model to address these concerns and obtained good results.

A more recent paper by Facchinetti, *et al.* [58] reviews wake oscillator models for VIV. It examines the effects of using three different mechanisms to couple the wake and structural equations: displacement coupling, velocity coupling, and acceleration coupling. These methods operate by applying either the displacement, velocity or acceleration response from the structural equation as forcing to the wake equation. The coupling is completed by using the displacement response from the wake equation to force the structural equation. It was found that displacement coupling fails to predict the lift caused by vortex shedding, the lift magnification at lock-in, and all significant features of VIV at Skop-Griffin (SG) numbers below 1.7. The dimensionless Skop-Griffin number characterizes the mass and damping of a structure and is defined as

$$SG = 8\pi^2 St^2 \mu^2 \zeta, \tag{4.1}$$

where μ is a non-dimensional mass and ζ is the structural damping ratio. Velocity coupling also fails to model the lift force due to vortex shedding and does not capture the full lock-in range at low values of SG. Acceleration coupling, however, was found to model most features of VIV of a cylinder in flow.

The Facchinetti, *et al.* [58] model was further enhanced by Xu, *et al.* [63] who introduced a method of estimating the empirical parameters found in the wake oscillator equation. Another modification of the wake oscillator model was proposed by Farshidianfar and Zanganeh [64] to better model the system response at low mass-damping ratios. They used a second van der Pol equation to model the structure and used velocity coupling. For a more comprehensive overview of VIV of circular cylinders see Gabbai and Benaroya [65].

4.2 Model

Consider a bellows joint with an arbitrary number of convolutes, denoted N_c. The parameters defining convolute geometry are shown in Fig. 2.1. Here, the Facchinetti, *et al.* [58] cylinder VIV model is adapted to an arbitrary bellows configuration by modeling the bellows joint as a spring-mass-damper system, with each mass representing a single convolute as shown in Fig. 4.1. This differs somewhat from the model used in TM-82556 where each half of a convolute represented a single mass.

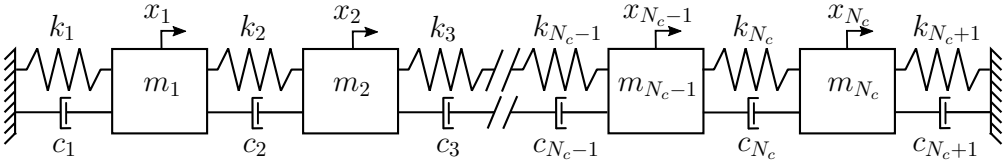

Figure 4.1: Spring-mass-damper diagram for coupled oscillator model

This leads to a system of N_c structural equations of motion given by

$$[M]\{\ddot{x}\} + [C_s + C_{fl}]\{\dot{x}\} + [K]\{x\} = \{F\} \tag{4.2}$$

where x is the structural displacement.

The mass matrix [M] is a diagonal matrix with elements $m_s + m_{fl}$. The mass terms are calculated by adapting Eqs. (3.2) and (3.3) for use over a single convolute by including a multiple of two, resulting in equations:

$$m_s = 2\pi\rho_s D_m t N_p(\pi a + h - 2a), \tag{4.3}$$

and

$$m_{fl} = 2\left(B_1 m_{fl_1} + B_2 m_{fl_2}\left(\frac{n}{N_c}\right)\right), \tag{4.4}$$

where $n = 1 \ldots N_c$ is the mode number.

The stiffness matrix, $[K]$, is given by

$$[K] = \begin{bmatrix} k_1 + k_2 & -k_2 & 0 & \cdots & 0 \\ -k_2 & k_2 + k_3 & -k_3 & & \vdots \\ 0 & -k_3 & \ddots & -k_{N_c-1} & 0 \\ \vdots & & -k_{N_c-1} & k_{N_c-1} + k_{N_c} & -k_{N_c} \\ 0 & \cdots & 0 & -k_{N_c} & k_{N_c} + k_{N_c+1} \end{bmatrix}, \tag{4.5}$$

where $k_n = N_c K_a$. The overall stiffness, K_a, can either be found experimentally, calculated using Eq. (3.6) or by using another method discussed in Section 2.1.

The structural and fluid damping matrices, $[C_s]$ and $[C_{fl}]$, have the same structure as $[K]$ in Eq. (4.5). If desired, the damping coefficient elements, c_s, can be chosen to yield a known viscous modal damping ratio. The fluid damping elements, c_{fl}, are given by

$$c_{fl} = \frac{1}{2}\rho_{fl} h w U C_D, \tag{4.6}$$

where w is the circumference of the bellows at the mean diameter and C_D is a drag coefficient that captures the resistance of the fluid to convolute motion. The right hand side of Eq. (4.2)

represents the fluid force on the convolutes. This force is analogous to the fluctuating lift force on a cylinder experiencing VIV [58] and is described by

$$F = \frac{1}{2}\rho_{fl} h w U^2 C_f, \tag{4.7}$$

where C_f is a fluid force coefficient for a moving convolute.

The structural equations are coupled to a system of N_c fluid oscillator equations via the structural acceleration $\ddot{x_j}$ and are given by

$$\ddot{q_j} + 2\pi St \frac{U}{\lambda}\epsilon(q_j^2 - 1)\dot{q_j} + \left(2\pi St \frac{U}{\lambda}\right)^2 q_j = \frac{A}{\alpha}\ddot{x_j}, \tag{4.8}$$

where $j = 1 \ldots N_c$ for N_c fluid oscillator equations per bellows, St is the Strouhal number given by $St = f_{fl}\lambda/U$, f_{fl} is the frequency of the oscillating shear layer, ϵ is a parameter that determines the strength of the non-linear damping and A is a coupling force scaling parameter described in Facchinetti, *et al.* [58]. When $q < 1$, negative damping exists creating a dynamically unstable system that increases amplitude response. When $q > 1$, positive damping limits the amplitude response of the system. When the forcing term on the right hand side of Eq. (4.8) is zero and $0 < \epsilon \ll 1$ the equation will produce an oscillation with a finite amplitude of $q = 2$ [66]. The dimensionless fluid degree of freedom q is a reduced forcing coefficient representing the fluctuating pressure amplitude on a convolute and is defined as $q \equiv 2C_f/C_f^o$, where C_f^o is the coefficient calculated for a rigid convolute experiencing fluctuating fluid forcing. The force, F, acting on the structure can now be defined as

$$F_j = \left(\frac{\rho_f h w U^2}{2}\right)\left(\frac{C_f^o}{2}\right) q_j, \tag{4.9}$$

where q acts to couple the fluid oscillator, Eq. (4.8), to the structural oscillator, Eq. (4.2).

4.3 Model Inputs and Characterization

The model contains several parameters, namely: C_f, C_D, A, and ϵ, that need to be carefully chosen. Through a combination of literature surveys, CFD simulations and experimental data, realistic values of these parameters have been determined for a range of typical bellows configurations.

4.3.1 Forcing Coefficient

Here the forcing coefficients for a rigid convolute, C_f^o, have been determined using a range of 2-D rigid CFD simulations of varying bellows configurations. The CFD software program ANSYS Fluent® was used for these simulations. To find C_f^o, a bellows 2-D cross section was modeled, as shown in Fig. 4.2 for Gerlach [14] bellows 102. The convolute section and adjacent walls were no-slip boundaries with the adjacent mesh satisfying a $y^+ < 1$ condition. The boundary opposite the convolutes is the centerline of the bellows cross section and was set as a slip wall. The mesh contained approximately two million elements with the greatest concentration being located in and around the convolute cavities. The Detached Eddy Simulation model with the SST $k-\omega$ turbulence solver [67] was used with second order discretization and double precision. Convergence criteria for the conservation equations was set to the order of 10^{-6}.

Data were collected for the fluid force on a convolute by calculating the pressure integral over the height of the upstream and downstream halves of a convolute with a unit depth. A similar approach was used by Gharib and Roshko [68] to calculate fluctuating fluid forces acting on rectangular cavities. The net fluid force, F_{fl_j}, per convolute is found by subtracting pressure integral time history of the upstream convolute half from the that of the downstream half. The fluid force coefficient for each convolute is then found using

$$C_f^o = \sqrt{2} RMS \left(\frac{2F_{fl_j}}{\rho_{fl} U^2 h} \right), \tag{4.10}$$

where $\sqrt{2}RMS$ is the root-mean square used to find the zero-to-peak amplitude of the resulting time history.

A partial time history and corresponding fast Fourier transform of the Gerlach [14] bellows 102 case with a flow velocity of 6.4 m/s is found in Figs. 4.3a and 4.3b. The dominate frequency for this sample case is 399 Hz. This frequency corresponds to an $St = 0.41$, which is near the range of $St = 0.42 - 0.50$ discussed in Section 2.6.1.

(a)

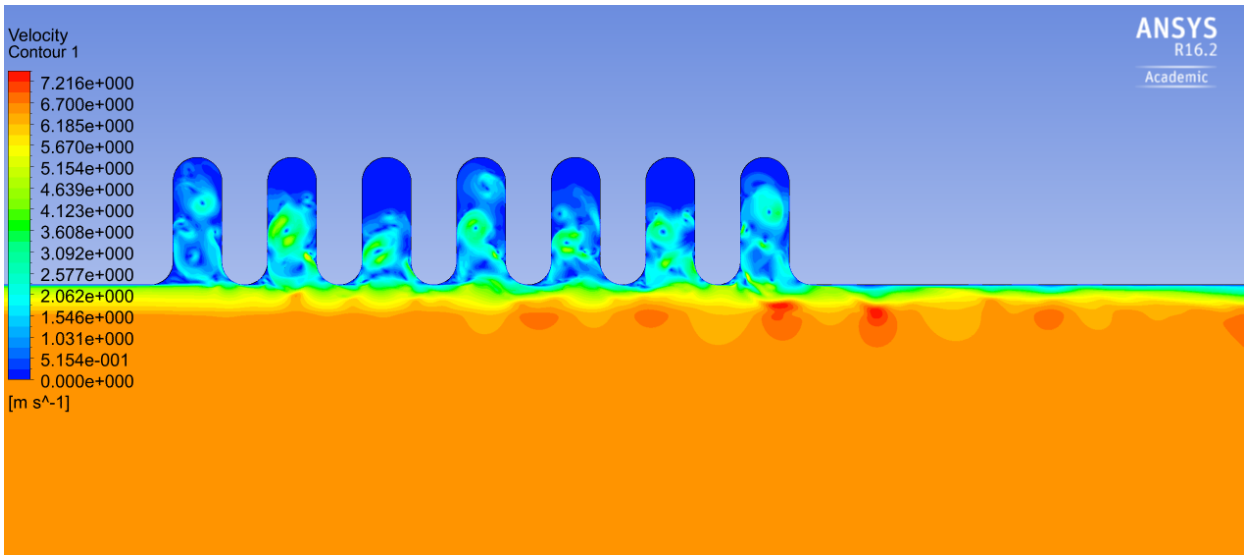

(b)

Figure 4.2: CFD velocity contour plot of Gerlach [14] bellows 102, (a) and detailed area, (b). Flow direction is from left to right with a 6.4 m/s velocity at the inlet.

Gerlach and his associates [12–14] developed the relationship between the dynamic C_f and λ/α, shown in Fig. 4.4a, using data from flow testing of a flexible ring that represented a single convolute. Simulations were conducted to study the affect of varying pitch/width has on C_f^o and the results are shown in Fig. 4.4b. The λ/h ratios and velocity were maintained for the simulations while convolute pitch and width were varied. The Gidi [42] geometry was used for the altered pitch and width cases. It is seen that C_f^o did not vary greatly with changing λ/α ratio as Gerlach's C_f curves would suggest in Fig. 4.4a.

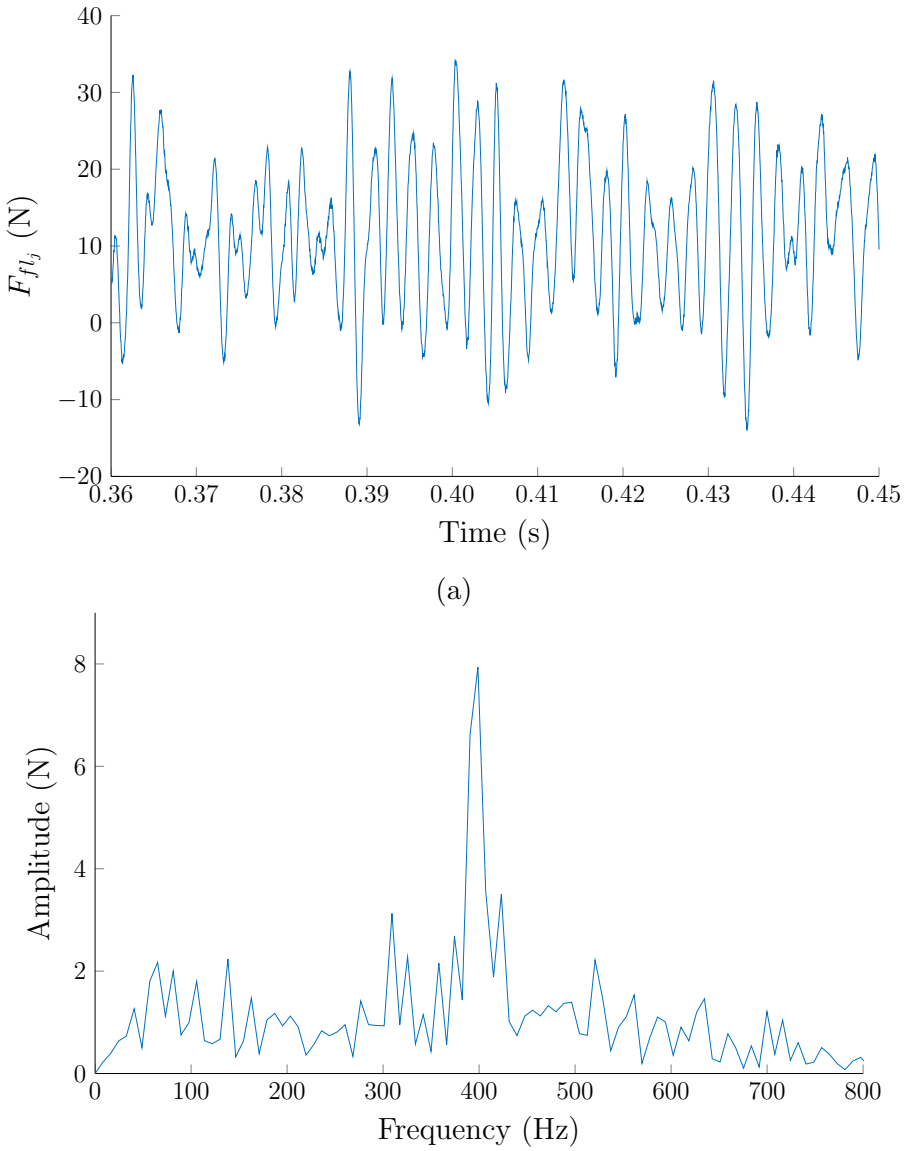

Figure 4.3: Partial CFD time history, (a), and corresponding Fast Fourier transform, (b), for the trailing wall of the third convolute of Gerlach bellows 102 geometry at a flow velocity of 6.4 m/s, frequency of 399 Hz and $St = 0.41$.

The results in Fig. 4.5 show that C_f^o increases with increasing convolute number, indicating a stronger forcing on downstream convolutes. Each data set in Fig. 4.5 represents a unique condition for seven bellows geometries. The Gidi [42] case is distinct in that the upstream and downstream edges of the outer convolutes have straight edges instead of U-shaped edges like all other bellows configurations examined in this study. The effect of the straight edge is pronounced for the first convolute where the C_f^o value is much higher than when compared to the same case with rounded edges. The Gidi geometry with rounded upstream and downstream edges was also modified from six to 16 convolutes to expand on the relation that C_f^o increases with convolute number.

Gerlach and Schroeder [13] bellows 102 and 105 share the same geometry, but differ by the flow velocities (6.4 m/s and 7.2 m/s) that excited the first mode. This is also the case for bellows 104 and 110 from the same report having excitation velocities of 9.5 m/s and 9.7 m/s. Bellows 106 varies greatly from all other configurations examined. This is explained by the bellows 106 convolutes being shallow cavities with a $\lambda/h = 1.5$, where as all other bellows examined are deep cavities having $\lambda/h < 1$. No more attention has been given to bellows having shallow cavity geometry.

From these results, excluding bellows 106 and straight edged Gidi geometries, estimates of C_f^o values per cavity for bellows of common, configurations can be based on the following curve fit found from Fig. 4.5:

$$C_f^o = -0.000176j^2 + 0.007991j - 0.002131, \tag{4.11}$$

where $j = 1 \ldots N_c$.

The relationship between C_f^o and increasing flow velocity was examined using a simulation that varied the inlet flow velocity from $0 - 10$ m/s using the Gerlach bellows 102 geometry. The results are shown in Fig. 4.6 for the first, third and seventh convolutes. The first convolute shows a steady C_f^o value, while the latter convolutes show increasing dispersion, likely caused by turbulence, and a decrease in C_f^o for increasing velocity. Figure 4.7 is a

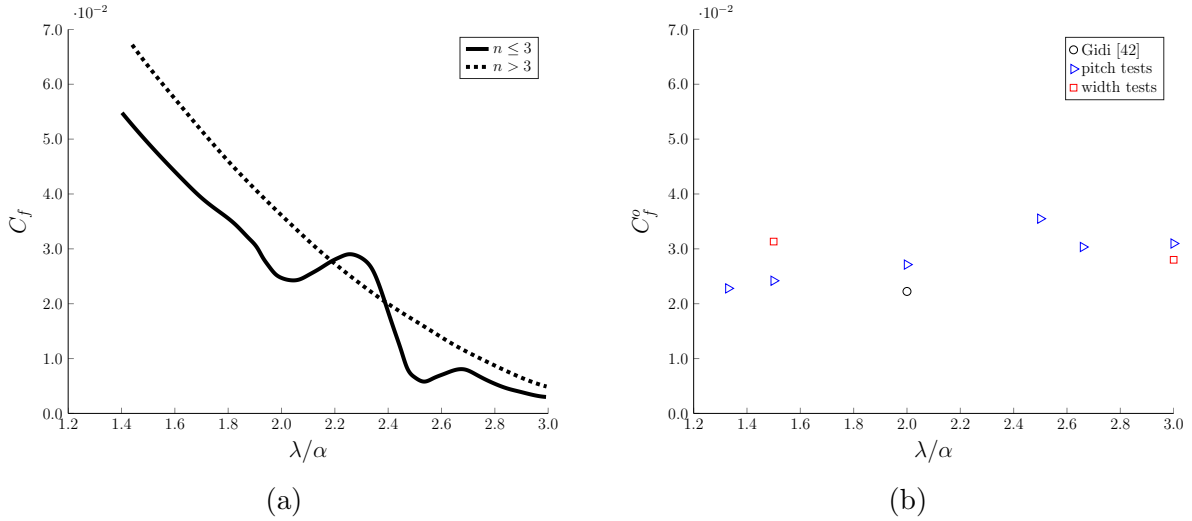

Figure 4.4: Gerlach and Schroeder [13] force coefficient, C_f, vs. pitch/height ratio, λ/α, for modes $n \leq 3$, —, and $n > 3$, - - -, (a), and the effect of changing pitch and width on C_f^o, (b).

spectrogram of the third convolutes' time history that shows the linear relationship between frequency and velocity. From this spectrogram and from those for the other convolutes not shown, the Strouhal number is found to be approximately $St = 0.41$ for all convolutes. This is close to the range found from experiments ($St = 0.42 - 0.50$) and provides some confidence in the CFD simulation. With these results, C_f^o can now be approximated for each cavity of a bellows joint using Eq. (4.11) without concern that changes in pitch and width will cause variations.

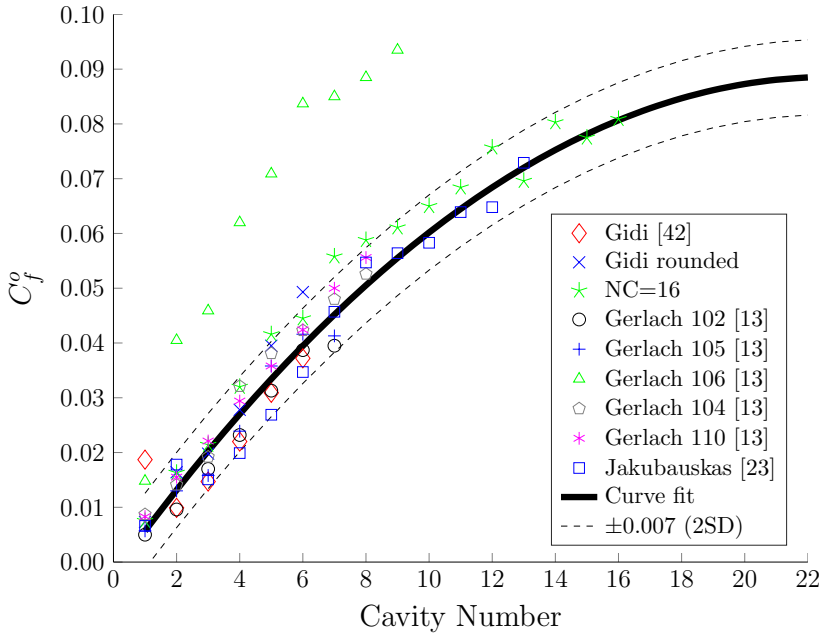

Figure 4.5: Forcing coefficient, C_f^o, as determined by 2-D rigid CFD simulations with curve fit (two standard deviations=±0.007, - - -).

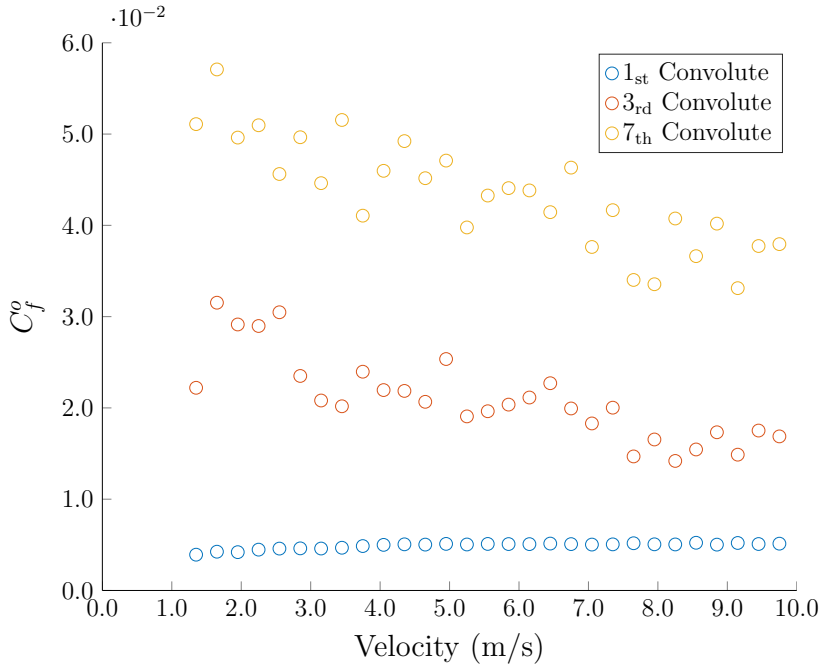

Figure 4.6: The effect of varying the flow velocity on the forcing coefficient, C_f^o, for the 1st, 3rd and 7th convolutes using the Gerlach and Schroeder [13] bellows 102 geometry.

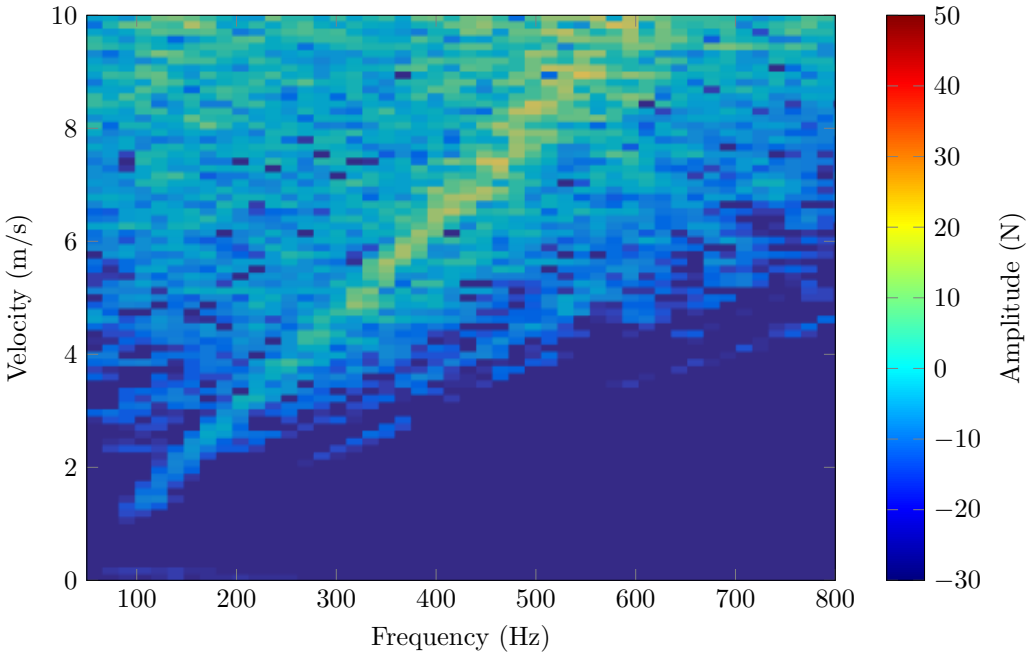

Figure 4.7: Spectrogram of the third convolute of Gerlach and Schroeder [13] bellows 102 geometry for increasing velocity.

4.3.2 Drag Coefficient

There does not exist experimental or theoretical data pertaining to the drag coefficient of bellows joints. It is assumed that the convolutes of a bellows joint vibrating in an axial mode are resisted by the fluid in a manner akin to a flat plate oscillating in fluid. Consulting literature regarding drag coefficients for flat plates in fluid, it was found that $C_D \approx 2$ is appropriate for flows with Reynolds numbers greater than 10^4 [69]. So $C_D = 2$ will be used for all simulations shown here.

4.3.3 Lock-in and A

A method for examining frequency lock-in is found among cylinder VIV literature; particularly from de Langre [70]. To gain insight into the nature of lock-in, we consider an undamped, coupled two degree-of-freedom system having the structural and fluid equations of motion

$$M\ddot{x}(t) + Kx(t) = \frac{1}{4}\rho_{fl} hw U^2 C_f^o q(t) \tag{4.12}$$

and

$$\ddot{q}(t) + \left(2\pi St \frac{U}{\lambda}\right)^2 q(t) = \frac{A}{\alpha}\ddot{x}(t). \tag{4.13}$$

The equations can then put into a dimensionless form using the variables

$$\tau = \sqrt{\frac{K}{M}}t, \quad X = \frac{x}{\lambda}. \tag{4.14}$$

Substituting the dimensionless variables in Eq. (4.12) it becomes

$$\lambda K\ddot{X}(\tau) + \lambda K X(\tau) = \frac{1}{4}\rho_{fl} hw U^2 C_f^o q(\tau). \tag{4.15}$$

Dividing through by λK and using the relation $K = 4\pi^2 f_s^2 M$ it now reads

$$\ddot{X}(\tau) + X(\tau) = \frac{\rho_{fl} h w U^2 C_f^o}{16\pi^2 f_s^2 \lambda M} q(\tau). \tag{4.16}$$

Multiplying by $\lambda St^2/\lambda St^2$ and defining the reduced velocity as $U_r = U/(\lambda f_s)$, the dimensionless structural equation is

$$\ddot{X}(\tau) + X(\tau) = \Gamma St^2 U_r^2 q(\tau), \tag{4.17}$$

where

$$\Gamma = \frac{\rho_f h w \lambda C_f^o}{16\pi^2 St^2 m_{fl}(m^* + 1)}, \tag{4.18}$$

and $m^* = m_s/m_{fl}$.

The fluid equation, Eq. (4.13), with dimensionless variables substituted, is

$$\frac{K}{M}\ddot{q}(\tau) + \left(2\pi St \frac{U}{\lambda}\right)^2 q(\tau) = A\frac{\lambda K}{\alpha M}\ddot{X}(\tau). \tag{4.19}$$

Dividing though by K/M, the dimensionless fluid equation simplifies to

$$\ddot{q}(\tau) + St^2 U_r^2 q(\tau) = A\frac{\lambda}{\alpha}\ddot{X}(\tau). \tag{4.20}$$

The product StU_r is a dimensionless frequency of the oscillating fluid that is proportional to the flow velocity.

To solve Eqs. (4.14) and (4.20), assume a solution is of the form $(X, q) = (X_o, q_o)e^{i\omega\tau}$ to find the characteristic equation:

$$\omega^4 + \left[\left(A\Gamma\frac{\lambda}{\alpha} - 1\right) St^2 U_r^2 - 1\right]\omega^2 + St^2 U_r^2 = 0. \tag{4.21}$$

Using the quadratic formula, Eq. (4.21) becomes

$$\omega^2 = \frac{1}{2}\left(1 - \left(A\Gamma\frac{\lambda}{\alpha} - 1\right)St^2U_r^2 \pm \sqrt{\left(\left(A\Gamma\frac{\lambda}{\alpha} - 1\right)St^2U_r^2 - 1\right)\omega^2 - 4St^2U_r^2}\right). \quad (4.22)$$

Considering a case where $A\Gamma\lambda/\alpha = 0.04$, since bellows configurations found in literature have an $A\Gamma\lambda/\alpha$ value ranging between 0.01-0.06, we can compute ω from Eq. (4.21) for increasing StU_r, as seen in Fig. 4.8a. It is recognized that when $StU_r < (1 + \sqrt{A\Gamma\lambda/\alpha})^{-1}$ and $StU_r > (1 - \sqrt{A\Gamma\lambda/\alpha})^{-1}$ two neutrally stable modes, the structural and fluid modes, exist with real frequencies [70]. A neutrally stable system, when acted upon, will neither become unstable or return to its exact previous state. Examining Fig. 4.8a, the structural mode tracks along real $w_R = 1$, while the fluid mode follows closely to $\omega_R = StU_r$.

As StU_r increases, the fluid and structural frequencies merge together. This lock-in region is defined by $(1 + \sqrt{A\Gamma\lambda/\alpha})^{-1} < StU_r < (1 - \sqrt{A\Gamma\lambda/\alpha})^{-1}$ around $StU_r = 1$. Two modes exist in this region with complex conjugate frequencies, but one of the coupled modes is now damped and the other is unstable ($\omega_I < 0$), as shown in Fig. 4.8b. As StU_r continues to increase the two modes decouple and return to neutral stability. This behavior is analogues to the phenomenon of coupled-mode flutter [35, 70].

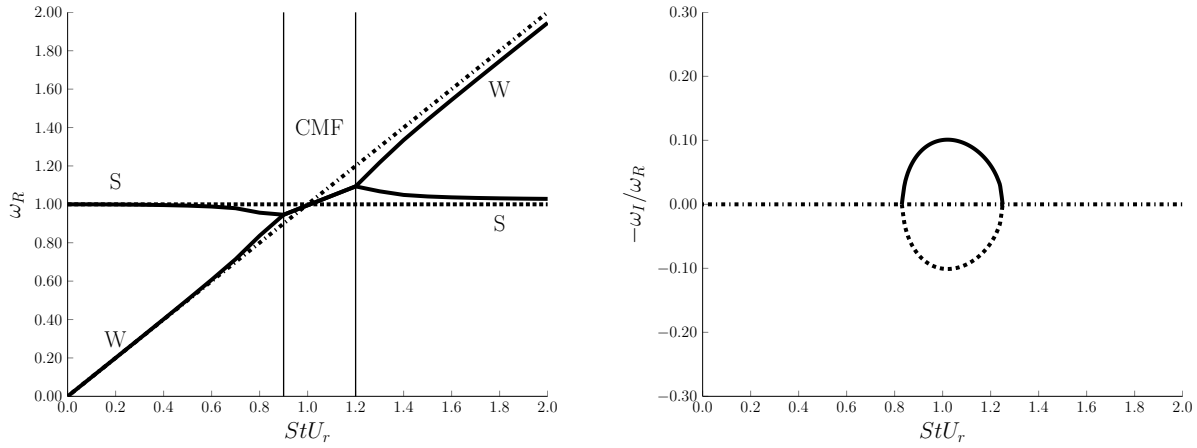

(a) Frequency (b) Growth rate

Figure 4.8: The effect of increasing StU_r on the (a) frequencies and (b) growth rate of the coupled system with $A\Gamma\lambda/\alpha = 0.04$. —, Unstable mode; - - -, damped mode; $\cdots$, uncoupled structural mode; - $\cdot$ -, fluid mode of uncoupled solution when $A\Gamma\lambda/\alpha = 0$ and $\omega_R = StU_r$. In (a), CMF shows the bounded coupled mode flutter region, S is the structural mode and W is the fluid mode.

The $A\Gamma\lambda/\alpha$ parameter is responsible for the magnitude of the lock-in range and the change in frequency. If $A\Gamma\lambda/\alpha < 1$, the two frequencies of the system corresponding to the fluid and structural modes can be tracked by varying StU_r, which determines the stability of the system. Figures 4.9a and 4.9b show how the lock-in region increases with increasing values of $A\Gamma\lambda/\alpha$. Interestingly, the upper bound of the lock-in range expands more quickly than the lower bound for increasing $A\Gamma\lambda/\alpha$; however, for the small values of $A\Gamma\lambda/\alpha$ found for bellows, the upper and lower bounds of the lock-in range are fairly symmetric.

With this technique lock-in region plots can be created for any bellows given C_f^o, St, geometry and material properties. Figure 4.10a shows the lock-in region of bellows flow experiments overlaid on the prediction created using the properties of Gerlach's bellows 102, (see Sections 4.3 and 4.4). The lock-in range of experimental data is plotted by finding the upper and lower velocity bounds at 60% of the peak amplitude response. For a typical bellows, Fig. 4.10a can be used to provide a quick estimate of the velocity range in which a given bellows is susceptible to FIV. This method is particularly useful as it can be used to determine the coupling force scaling parameter, A, by comparison with experimental data.

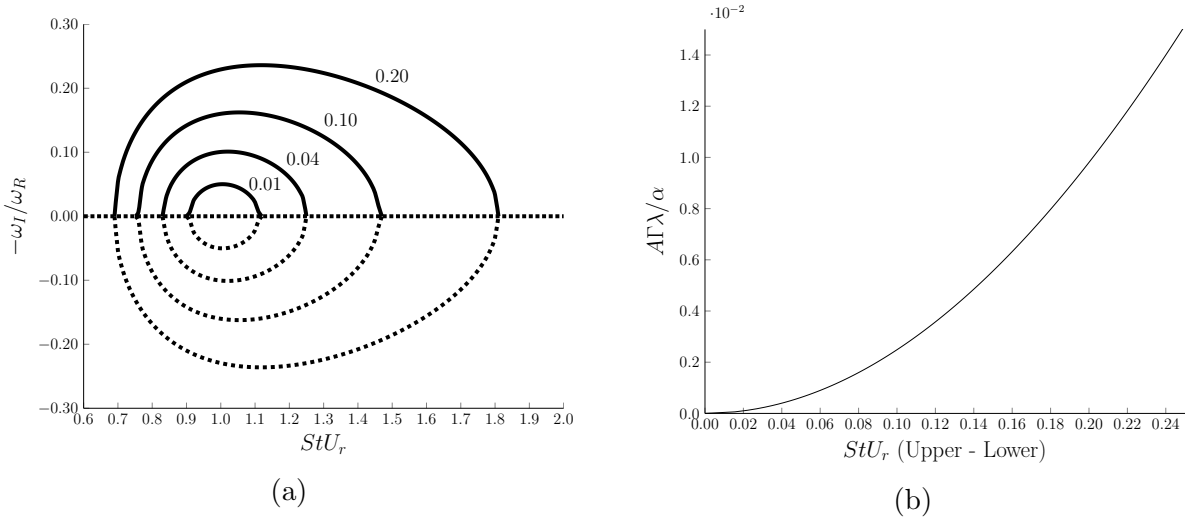

(a) (b)

Figure 4.9: (a), The effect of varying $A\Gamma\lambda/\alpha$ for values of 0.01, 0.04, 0.10 and 0.20 on the growth rate of the coupled system with $A\Gamma\lambda/\alpha = 0.04$. —, Unstable mode; - - -, damped mode; $\cdots$, fluid mode of uncoupled solution when $A\Gamma\lambda/\alpha = 0$ and $\omega_R = StU_r$ and, (b), the effect increasing $A\Gamma\lambda/\alpha$ has on the lock-in range (upper StU_r - lower StU_r).

Examining Fig. 4.10a, the data fit the trend of decreasing StU_r with increasing m^*; however, the model's bias towards higher StU_r values is not reflected by experimental data. In fact, the upper bound increases at a higher rate than the lower bound when A is increased. This behavior is also noted by de Langre [70]. Because of this, there are two potential methods for selecting A from this information. An A value could be chosen to align with the upper StU_r bound while under-predicting the lower bound or it could be chosen to capture the width of the lock-in region with the caveat that it is offset towards higher values of StU_r. In Table 4.1, the method of residual sum of squares (RSS) was used to evaluate both techniques for the first mode response of each bellows. In column I, an A value was selected to provide the smallest difference between the RSS for the upper and lower StU_r bounds for a given bellows. Column II values were calculated by selecting an A that gave the smallest RSS value for just the upper bound.

Examining Table 4.1, it is not a surprise that the quasi-2D geometry of the Gidi case has different A values than actual bellows and the result for bellows 106 is not unexpected

Table 4.1: Comparison of A values for each bellows found using: I, the difference of the upper and lower bound RSS; II, just the upper bound RSS

Bellows	**I**	**II**
Gidi Exp. 6 [42]	5.5	2.9
Gerlach and Schroeder 102 [13]	22.6	17.6
Gerlach and Schroeder 104 [13]	21.0	18.3
Gerlach and Schroeder 105 [13]	13.6	8.5
Gerlach and Schroeder 106 [13]	2.8	1.4
Gerlach and Schroeder 110 [13]	13.0	6.0
Bass and Holster 3 [15]	19.9	6.1
Bass and Holster 6 [15]	25.3	13.3
Jakubauskas and Weaver [23]	20.5	13.2

either as it has an atypical geometry when compared with the other specimens, see Table 4.3. There is not much variation in A for each method. Typical A values range between 13.0-25.3 for column I and it would require a much larger change in A to significantly affect the lock-in region. Excluding the Gidi cases and bellows 106, the RSS method provides a best fit to the lock-in width using an $A = 19.1$ for standard, deep cavity bellows. In contrast, if the fit to only the upper StU_r bound is used, a value of $A = 11.8$ is found. Rounding up and choosing an $A = 20.0$ is the conservative choice since the larger lock-in range better fits the experimental data and an overestimation would be preferred. Figures 4.10a-4.10c show the predicted lock-in regions for bellows 102, the Gidi experiment 6 case and the bellows 106 case with their respective A values. Figure 4.10a is representative of typical bellows geometries and has a similar lock-in region to the other experimental data listed. For Figs. 4.10b and 4.10c an $A = 20$ was also plotted using their respective geometries to show how these two cases differ from other bellows.

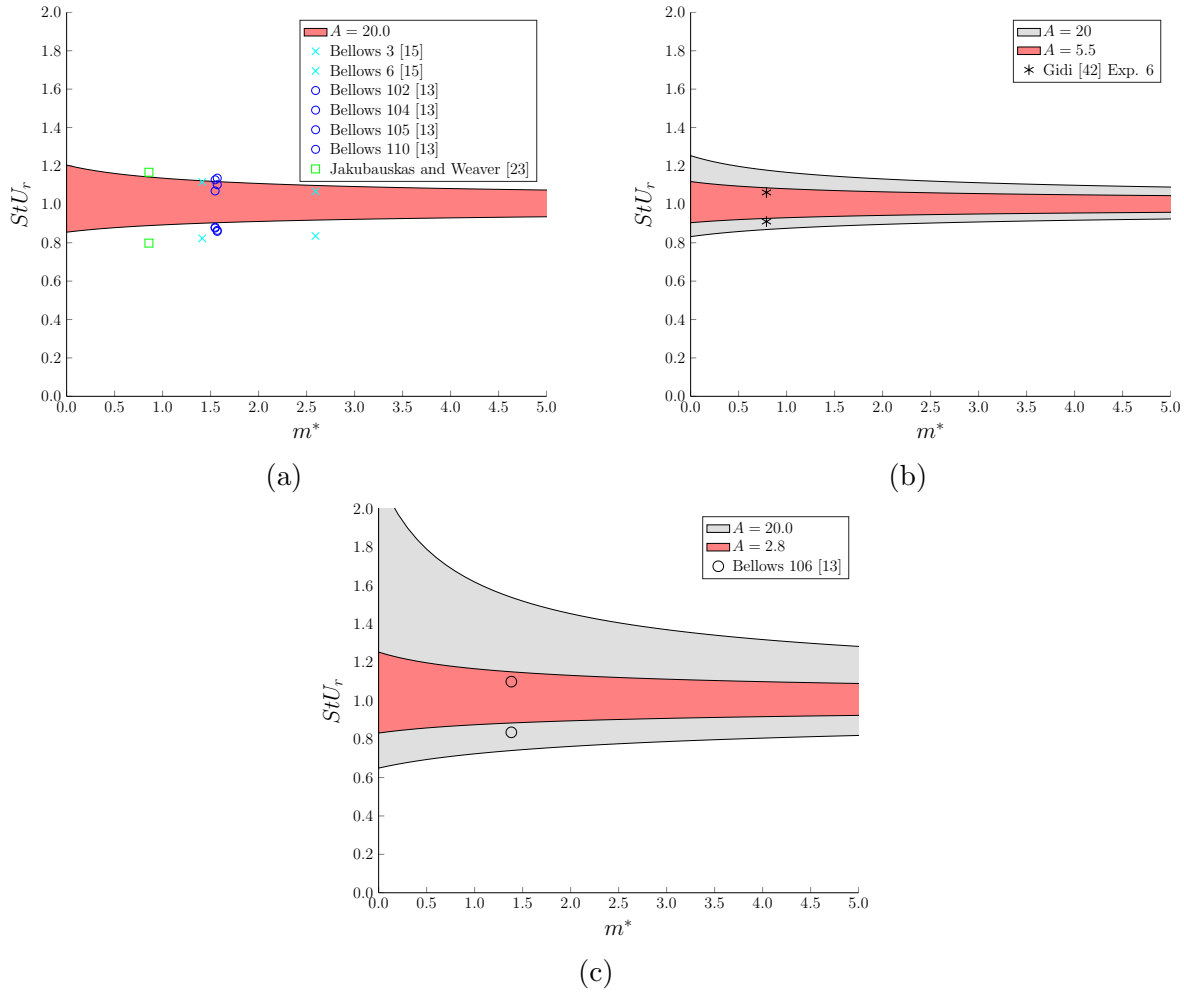

Figure 4.10: Lock-in range for (a) typical bellows, $A = 20$, (b) Gidi [42] quasi-2D bellows, $A = 5.5$, and (c) Gerlach and Schroeder [13] bellows 106, $A = 2.8$

4.3.4 Van der Pol Parameter

Having determined representative A values, a basis for selecting the the van der Pol parameter, ϵ, can be found in cylinder VIV literature. Facchinetti, *et al.* [58] proposed a ratio of $A/\epsilon = 40$ based on a fit to experimental data for which they compared the lift magnification factor resulting from an imposed structural amplitude. There are not computational or experimental data available to determine if this ratio is similar for bellows systems. In the absence of these data, a A/ϵ ratio of 40 is also used here.

4.4 Model Results and Validation

Since bellows joints are often critical system components, any mathematical model should be carefully validated. The data available from the water flow testing by NASA [5] and SwRI [16] are mostly represented in terms of strain, but there are a few data sets that can be compared with the model's prediction. Gidi [42] collected amplitude and flow velocity data with a quasi-2D bellows flow experiment. It is particularly useful as amplitude data was reported for each convolute. The model is also used to construct a design chart for predicting maximum amplitude response.

4.4.1 Gidi Experiments

Gidi's [42] data were presented in his thesis and were also summarized in an article by Gidi and Weaver [41]. He built a quasi 2-D model of a bellows joint and placed it in a water flow loop. The model geometry was upscaled from an actual bellows tested by Weaver and Ainsworth [40] to compare the results with the FIV characteristics of the parent model. It can be described as an "extruded" 2-D cross section of of a bellows consisting of five convolute-shaped acrylic blocks supported on long aluminum rods. Springs were attached between the rods to simulate elastic coupling between the convolutes. Thin mylar strips were attached at the base of the acrylic blocks to form the cavity geometry of a bellows joint. The five convolute assembly was attached to a base plate and placed in the test section such that the tips of the convolutes were at the same height as the upstream and downstream edges of the test section. The convolutes could also be raised or lowered to change the flow impingement points. This model was particularly unique because transparent side walls allowed for flow visualization. Amplitude response data were gathered by attaching a strain gauge at the base of each rod.

In Gidi's sixth experiment, the maximum response of the first mode occurred at a frequency of 2.5 Hz with a flow velocity of about 0.5 m/s, an $St = 0.45$ and a corresponding

Reynolds number of approximately 44,000. These values can also be found in Table 4.5. The two outermost spring constants were $k_e = 1.49$ kN/m and the inner spring constants were $k_i = 0.88$ kN/m. Gidi cited a fluid mass of 0.657 kg per convolute; however, calculations show that it should be 0.701 kg for the fluid mass surrounding the inner convolutes and the outer convolutes have an additional 0.291 kg of fluid mass each. All other geometric and material properties can be found in Tables 4.3 and 4.4. Other values used are $A = 5.5$, $\epsilon = 0.1375$, $C_D = 2$ and $c_s = 0.69$. The structural damping coefficient element, c_s, was selected by applying the log decrement method to the uncoupled structural equation and adjusting c_s until $\zeta = 0.005$. The forcing coefficients were determined via CFD simulation to be $C_f^o = [0.0187, 0.0099, 0.0147, 0.0220, 0.0309]$. In addition to applying this convolute specific forcing coefficient to the model, it's average, $C_f^o = 0.0192$, and the average of the values calculated using Eq. (4.11), $C_f^o = 0.0184$, are compared. The coupled oscillator model was programmed using the ODE45 solver in Matlab® to calculate convolute amplitude response results for the geometry and flow conditions corresponding to the first mode of the sixth Gidi experiment [42]. The frequency of this mode was predicted by the model to be $f_s = 2.52$ Hz while the experiment demonstrated a corresponding frequency of $f_s = 2.50$ Hz.

Experimental and predicted convolute amplitude responses are shown in Fig. 4.11 where $|x|/\alpha$ is the amplitude response normalized by the convolute width. As shown in Figs. 4.11b - 4.11d, the predicted response curves using the convolute specific C_f^o values are within 16% of the experimental amplitude results for the inside convolutes and within 7% when the average of the convolute specific C_f^o is used. The $C_f^o = 0.0184$ falls in between the other two methods and within 10% of the experiment.

The outer convolutes are under-predicted by at most 57%. The first mode shape of the structural system is [0.3651, 0.8262, 1.0000, 0.8262, 0.3651], where the maximum modal amplitude has been normalized to one. This mode indicates that the maximum amplitude response of the outer convolutes will be approximately 36% of the center convolute for the model, but the experimental results indicate that the amplitude of the outer convolutes were

69% of the center convolutes' amplitude. Gidi does note that since the outer cavities have a fixed wall, the rate of volume change in the outer cavities are not the same as that for the inner cavities and could affect the system [42]. A better explanation for this behavior is not available and it is assumed to be an eccentricity of this particular experimental system.

Figure 4.11f shows the frequency lock-in region for the convolute specific CFD case. Taking the lock-in region to be the lower and upper velocity values at 60% of the peak amplitude, denoted by the shaded area, the model indicates lock-in occurring over a tight range of flow speeds ($StU_r = 0.95 - 1.06$) with a 32.4% difference in width between the model and experiment. This improves to a 23.7% difference for $C_f^o = 0.0192$. It also seems to exhibit a slight asymmetry with the lock-in region biased to $StU_r > 1$. The slope of the model's prediction for f_{fl}/f_s in the lock-in range is only slightly perturbed, indicating that the degree of lock-in is small. The predicted flow velocity at peak amplitude for all three methods is 0.51 m/s; very close to the experiment's 0.5 m/s.

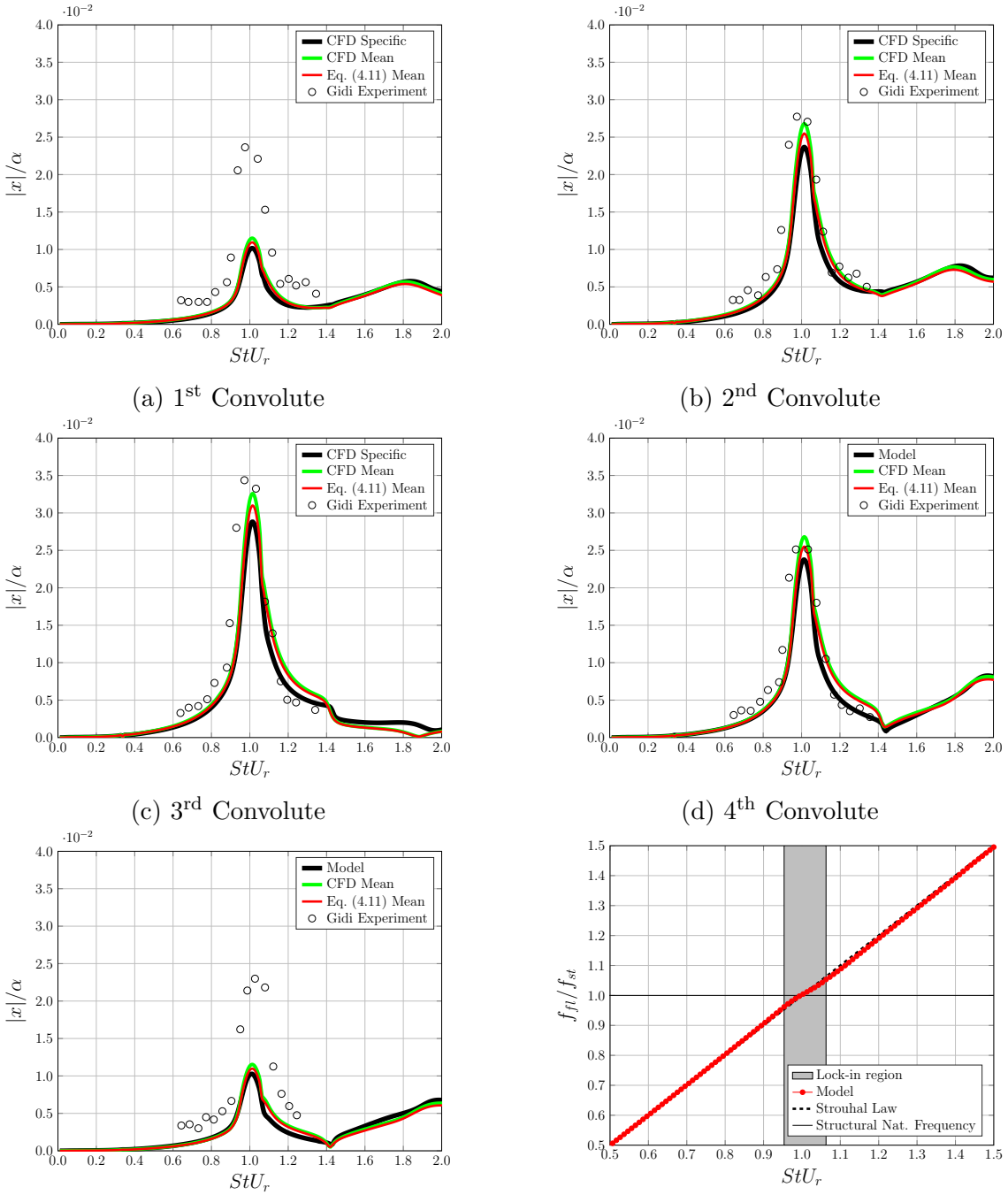

(a) 1st Convolute

(b) 2nd Convolute

(c) 3rd Convolute

(d) 4th Convolute

(e) 5th Convolute

(f) Lock-in region

Figure 4.11: (a)-(e), Normalized amplitude response of convolutes versus reduced frequency times Strouhal number for Gidi's sixth experiment [42] using convolute specific CFD, average CFD, and Eq. (4.11) derived C_f^o values and, (f), the predicted frequency lock-in region for convolute 3 using CFD specific C_f^o.

4.4.2 SwRI Bellows Trials

The technical report by Gerlach and Schroeder [13] prepared for NASA by the Southwest Research Institute, along with the corresponding journal article by Gerlach [14], detail three tests that can be compared with the presented model: bellows tests 102, 104 and 105. The experimental data are in terms of strain, but a strain-to-displacement conversion factor was provided. In the experiments, displacement was calculated by attaching strain gauges to the crown of an end convolute and applying static loads to create a strain-deflection curve. Then, using the measured peak stain, S, from flow experiments and the slope of the strain-deflection curve, dS/dx, the displacement could be found using

$$x = \frac{S}{2N_c}\left(\frac{dS}{dx}\right)^{-1}. \tag{4.23}$$

This equation is used to convert the model's displacement result to strain for comparison with the experimental data in its native format.

The following values are used for all three bellows calculations: $A = 20$, $\epsilon = 0.5$, $St = 0.45$ and $C_D = 2$. Elements of the structural damping coefficient matrix $[C_s]$ are chosen for each bellows by adjusting their value until $\zeta = 0.005$ was found using the log decrement method on the uncoupled structural equation, resulting in c_s values of 7.14, 4.49, and 7.82 for bellows 102, 104 and 105 respectively. All other geometric, mass and flow properties can be found in Tables 4.3—4.6. The authors of the experimental data note that the reported geometries are only a representation and that the actual dimensions may vary slightly [13].

The bellows 102 experiment yielded a frequency of 478 Hz compared to the models predicted frequency of f_s=402 Hz for the first mode. A frequency of 440 Hz was predicted for bellows 105 versus the experimental frequency of 515 Hz for the first structural mode. For bellows 104, the experimental frequency was 813 Hz. Since a value for stiffness was not provided for bellows 104, Eq. (3.6) was used to predict a frequency of 537 Hz. To compensate for this large error, an overall stiffness value of $K_a = 283,000$ N/m was input

into the model to match the experimental frequency for the first axial mode. The CFD results for each bellows yielded peak frequencies of 409 Hz, 677 Hz and 478 Hz over each bellows first convolute respectively; however, the frequencies did decrease for downstream convolutes.

Three methods to apply the C_f^o values to the model are used. First, the CFD derived convolute specific C_f^o values are applied to each respective convolute and can be found in Table 4.6. Second, the average of the CFD derived C_f^o values are used. Lastly, Fig. 4.5 and Eq. (4.11) are used to determine an average C_f^o to apply to the model. Amplitude response, in terms of strain and StU_r, and frequency lock-in are plotted for each method in comparison with experiment and are shown in Fig. 4.12. The Strouhal numbers used to normalize the experimental results are found in Table 4.5. Additionally, the percent difference between the model and experiment for three parameters—peak amplitude, lock-in width and velocity at peak amplitude—are shown in Table 4.2.

Examining the results of using the first method, shown in Fig. 4.12, the model over-predicts the amplitude response by about an average of 88% difference. The widths of the lock-in regions and the velocities at peak amplitude have a close fit to the experiment with average percent differences of just 9.8% and 5.6% respectively. Using average C_f^o values of 0.0235, 0.0319, 0.0253, for bellows 102, 104 and 105 respectively, provides nearly identical results. For amplitude and excitation velocity there was less than a 3% change and an 8% change for lock-in width.

For the final method, Eq. (4.11) provided average C_f^o values 0.0263, 0.0293 and 0.0263 for each bellows respectively. The results have just a slightly higher percent difference in comparison with experiment for all three parameters, as shown in Table 4.2. It does differ from the convolute specific, CFD derived C_f^o results by as much as 13% as seen for bellows 102's peak amplitude. The change in lock-in width is less than 5% and peak excitation velocity less than 2%. These results show that it appropriate to use Fig. 4.5 and Eq. (4.11) to select an average C_f^o value and apply it to the model.

While the predicted amplitude response is high, the accuracy of predictions for the lock-in width and peak amplitude velocity is very encouraging. Being able to pinpoint the peak excitation flow velocity and predict the onset and range of FIV in the first mode is a unique capability.

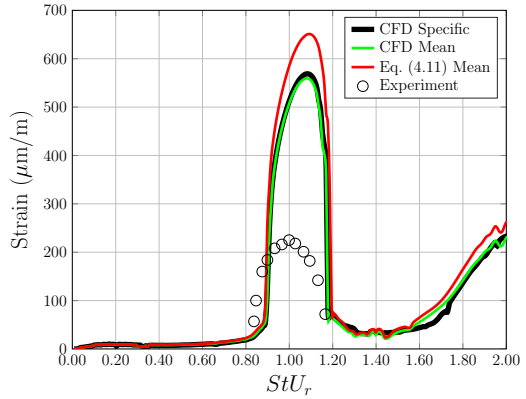

(a) Bellows 102

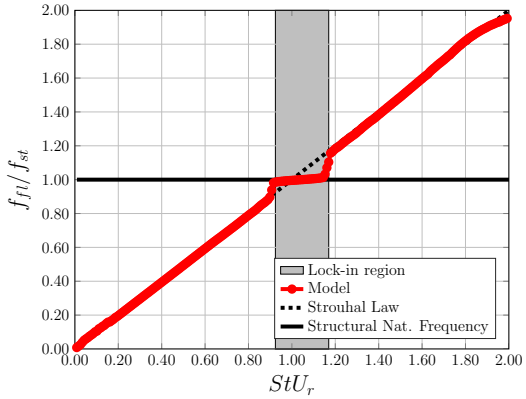

(b) Bellows 102

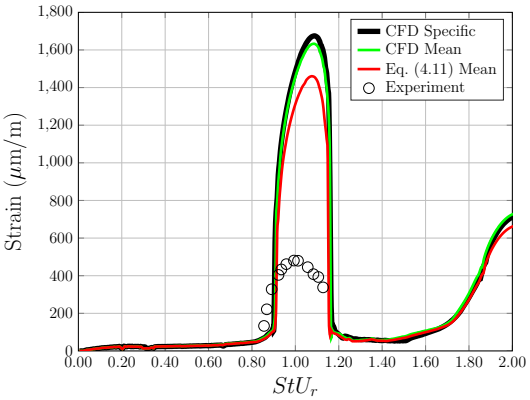

(c) Bellows 104

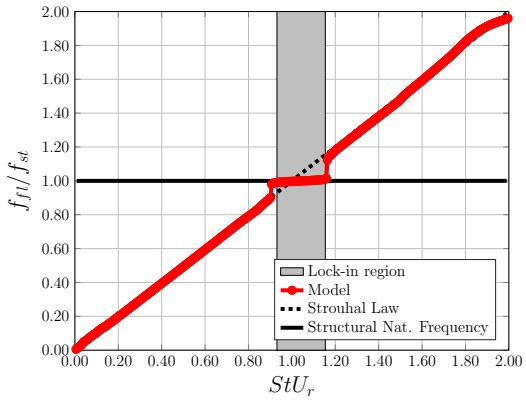

(d) Bellows 104

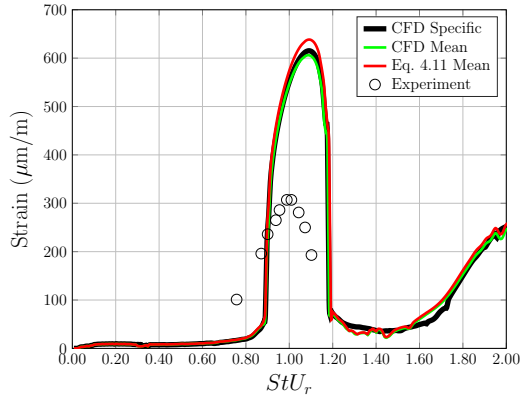

(e) Bellows 105

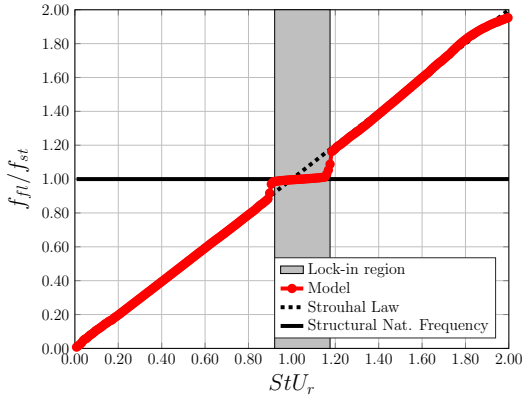

(f) Bellows 105

Figure 4.12: Gerlach and Schroeder [13] bellows 102, 104 and 105 amplitude responses for convolute specific CFD, average CFD, and Eq. (4.11) derived C_f^o values, (a), (c) and (e), and frequency lock-in regions, (b), (d) and (f) respectively for convolute specific, CFD derived C_f^o values.

Table 4.2: Percent difference between model and experiment for different C_f^o input methods: convolute specific CFD values, mean of CFD derived values, and mean of values found using Eq. (4.11).

Method	**Parameter**	**102**	**104**	**105**	**Mean**
CFD Specific	Amplitude	86.6	110.8	66.8	88.1
	Lock-in width	12.1	10.1	7.1	9.8
	Velocity	0	14.6	2.1	5.6
CFD Mean	Amplitude	86.6	109.1	65.5	86.6
	Lock-in width	12.1	7.9	7.1	9.1
	Velocity	0.8	14.2	2.1	5.7
Eq. (4.11) Mean	Amplitude	97.2	101.0	70.1	89.4
	Lock-in width	8.7	14.7	10.1	11.2
	Velocity	0.8	13.7	2.1	5.5

Table 4.3: Bellows geometric properties with all dimensions in centimeters

Bellows	N_c	D_m	λ	α	h	w	t
Gidi Exp. 6 [42]	5	-	9.0	4.5	13.5	9.6	-
Gerlach 102 [42]	7	4.6990	0.6604	0.31750	0.8890	14.76	0.03302
Gerlach 104 [42]	8	4.4196	0.5588	0.36576	0.6858	13.88	0.03302
Gerlach 105 [42]	7	4.6990	0.6604	0.31750	0.8890	14.76	0.03302
Gerlach 106 [42]	9	5.4864	0.6096	0.24130	0.4064	17.24	0.01524
Gerlach 110 [42]	8	4.4196	0.5588	0.36576	0.6858	13.88	0.03302
Bass and Holster 3 [15]	8	4.4196	0.5588	0.22606	0.6858	13.88	0.03302
Bass and Holster 6 [15]	7	4.699	0.6350	0.35052	0.8763	14.76	0.03302
Jakubauskas and Weaver [23]	13	16.84	1.202	0.7428	1.57	52.90	0.03680

Table 4.4: Bellows material properties

Bellows	m_s (kg)	m_{fl} (kg)	ρ_s (kg/m^3)	K_a(N/m)
Gidi Exp. 6 [42]	0.5221	0.6570	-	see text
Gerlach 102 [42]	0.0081	0.0052	7916.5	79508
Gerlach 104 [42]	0.0064	0.0041	7916.5	-
Gerlach 105 [42]	0.0081	0.0052	7916.5	95444
Gerlach 106 [42]	0.0023	0.0016	7916.5	-
Gerlach 110 [42]	0.0064	0.0041	7916.5	-
Bass and Holster 3 [15]	0.0058	0.0018	8000	-
Bass and Holster 6 [15]	0.0082	0.0047	8000	-
Jakubauskas and Weaver [23]	0.0604	0.0704	7860	43308

Table 4.5: Bellows flow properties

Bellows	$\boldsymbol{U}$ (m/s)	$\boldsymbol{St}$ (-)	**Reynolds # (-)**
Gidi Exp. 6 [42]	0.50	0.45	44,900
Gerlach 102 [13]	6.4075	0.493	42,200
Gerlach 104 [13]	9.5162	0.4774	53,100
Gerlach 105 [13]	7.2454	0.4694	47,800

Table 4.6: Gidi [42] and Gerlach and Schroeder [13] bellows forcing coefficients

Bellows	$\boldsymbol{C_f^o}$
Gidi Exp. 6 [42]	0.0187, 0.0099, 0.0147, 0.0220, 0.0309
Gerlach 102 [13]	0.0050, 0.0096, 0.0170, 0.0232, 0.0313, 0.0387, 0.0395
Gerlach 104 [13]	0.0087,0.0141, 0.0192, 0.0321, 0.0381,0.0423, 0.0480, 0.0526
Gerlach 105 [13]	0.0057, 0.0130, 0.0158, 0.0239, 0.0358, 0.0416, 0.0413

4.4.3 Self-Limiting Amplitudes

The proposed model can be used to predict maximum convolute response across a range of design parameters. Figure 4.13 shows the predicted maximum amplitude response of an end convolute normalized by convolute width, α, in the first mode for the Gerlach and Schroeder [13] bellows 102 geometry. The amplitudes are plotted against SG, defined by

$$SG = 8\pi^2 St^2 \mu^2 \zeta, \tag{4.24}$$

where μ is a nondimensional mass given by

$$\mu = \frac{m_s + m_{fl}}{\rho_f h w \lambda}. \tag{4.25}$$

The comparison is constructed by stepping the model through varying ζ values for different mean forcing coefficients, C_f^o. As a consequence of the self-limiting behavior of the model, the maximum amplitudes remain relativity constant for SG numbers less than one-half. These curves can be used as a design tool to estimate the maximum response for a given bellows geometry and structural damping.

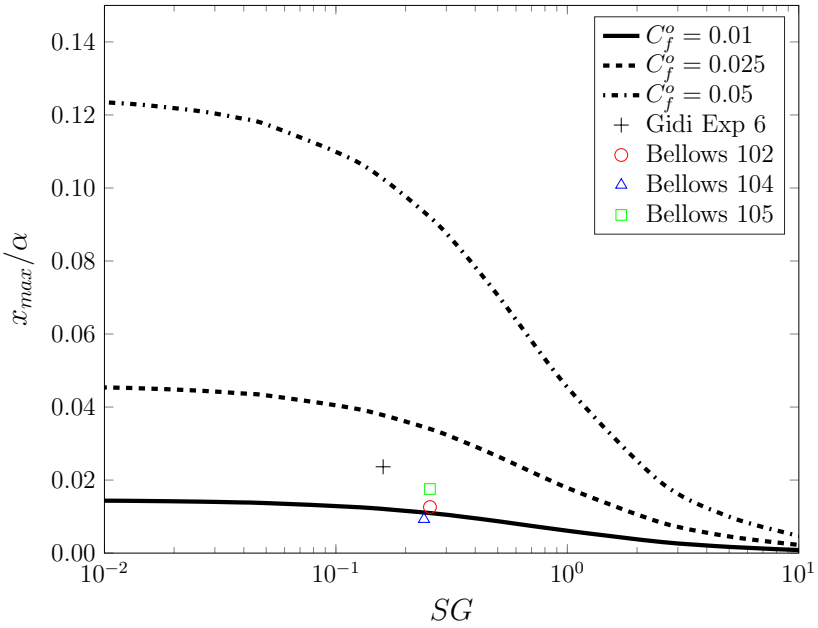

Figure 4.13: Normalized convolute amplitude versus SG for different values of fluid force coefficient, C_f^o. Data for Gidi [42] experiment 6, bellows 102, 104, and 105 [13] end convolute displacement is shown.

4.4.4 Model Application

To quickly estimate the maximum displacement in the first mode for a single-ply bellows the following parameters are needed: C_f^o, bellows geometric and material properties and the flow conditions. First, knowing the number of convolutes N_c, the average C_f^o can be calculated using

$$C_f^o = \frac{1}{N_c}\sum_{j=1}^{N_c}(-0.000176j^2 + 0.007991j - 0.002131). \tag{4.26}$$

Then the Skop-Griffin parameter SG is found with

$$SG = 8\pi^2 St^2 \mu^2 \zeta, \tag{4.27}$$

where the Strouhal number is $St = f_{fl}\lambda/U$, ζ is the damping ratio having typical values around 0.005 for a single-ply bellows, and μ is a nondimensional mass given by

$$\mu = \frac{m_s + m_{fl}}{\rho_f h w \lambda}. \tag{4.28}$$

Then with C_f^o and SG, Fig. 4.13 can be used to estimate the maximum amplitude response in the first mode. Presently, this is only valid for single-ply bellows, but similar design charts could be created in the future for multi-ply bellows once their structural damping characteristics are known.

The lock-in range for a bellows can be calculated using

$$(1 + \sqrt{A\Gamma\lambda/\alpha})^{-1} < StU_r < (1 - \sqrt{A\Gamma\lambda/\alpha})^{-1}, \tag{4.29}$$

where the coupling force scaling parameter is set to $A = 20$ for typical deep cavity, U-shaped bellows, α is the convolute root width, $U_r = U/f_s\lambda$ is the reduced velocity and Γ is defined as

$$\Gamma = \frac{\rho_f h w \lambda C_f^o}{16\pi^2 St^2 m_{fl}(m^* + 1)} \tag{4.30}$$

with $m* = m_s/m_{fl}$.

To obtain a more accurate prediction of amplitude response and lock-in region as well as velocity at peak excitation the model would need to be programmed to solve the system of $2N_c$ equations formed by Eqs. (4.2) and (4.8). At this time, it is recommended to use the TM-82556 method for calculating frequency, shown in Section 3.5, as it is currently more accurate than the model's prediction.

Chapter 5

Summary and Recommendations for Future Work

This investigation into flow-induced vibrations in bellows expansion joints has yielded notable contributions to the topic:

- This work contains the most comprehensive literature review of bellows joints that has been compiled. Discussions include surveys of axial and lateral natural frequency prediction methods, fluid-added mass predictions, stiffness calculations and modeling of flow-induced vibration.

- From more recent literature, it is apparent that the excitation mechanism acting on bellows involves free shear layer instabilities forming over the convolute cavities and not vortex shedding as was previously theorized. It has been shown that the characteristic length used to determine the oscillating fluid frequency of bellows should be the convolute pitch and not root width. This is akin to rectangular cavity driven oscillations. Examination of experimental results shows that the Strouhal number for bellows ranges between $St = 0.42 - 0.50$. A comparison has been made between cavity theory and data from bellows flow experiments that further supports this concept.

- The methods in TM-82556, used by NASA to predict bellows axial natural frequencies and flow-induced stresses, have been presented in new, nondimensional formats. This allows experimental axial natural frequency and stress data of bellows to be compared on a single plot. An expanded data set consisting of more than 120 entries from literature has been compared to the non-dimensional axial frequency prediction met-

hod, showing that is still quite accurate. Comparison of experimental data with the nondimensional formulation of the FIS method show that it is capable of approximately predicting stresses, provided that the specimens critical flow velocity, is near the predicted critical velocity. Procedures for using these methods have been outlined and should be a practical aid for designing and selecting bellows joints for a given operating environment.

- A new method for predicting bellows FIV has been developed. This method couples a discrete mechanical model of the bellows to a representation of the fluid wake expressed in terms of van der Pol oscillators. Inspired by a model of an elastically restrained, single degree-of-freedom cylinder in flow, it captures the salient physics of the bellows FIV phenomenon while remaining computationally efficient. The model has been shown to be capable of accurately predicting lock-in regions and flow velocities at peak excitation for the first mode of several experimental bellows found in literature. Convolute displacement and axial natural frequencies are also predicted. The coupled oscillator model separates itself from previous methods with the capability of accurately predicting the lock-in region over which excitation occurs. TM-82556 compensates for this by defining an overly large velocity range for resonant conditions, whereas the presented model is much more precise and is not as limiting from a design standpoint. Furthermore, the model is uniquely capable of predicting off-resonance conditions potentially allowing for more accurate fatigue life assessments.

- A design chart was also developed to predict maximum amplitude FIV response. The chart requires only an estimate of C_f^o and Skop-Griffin number as inputs.

- In development of the coupled oscillator model, forcing coefficients corresponding to rigid bellows, C_f^o, were determined using CFD simulations. It was found that C_f^o increases with increasing convolute number, while changes to convolute pitch and width had minor effects. A curve fit to these simulation results gives a design equation that

provides C_f^o values for each convolute in a bellows. When applying C_f^o to the model, it is sufficient to simply apply the average of the individual C_f^o values to all convolutes. Results from a CFD simulation that varied velocity show that as velocity increases, C_f^o is nearly constant for the first convolute, but can decrease with increasing velocity for downstream convolutes.

- A study was performed to examine the nature of frequency lock-in for bellows joints and to determine a value for the coupling force scaling parameter used in the van der Pol oscillator equations. It is shown that bellows lock-in is similar in nature to the coupled mode flutter phenomenon in which system frequencies merge together. The predicted lock-in regions for the bellows were compared with experimental results and it was found that an $A = 20$ provided the best fit for modeling the width of the lock-in range.

5.1 Recommendations for Future Work

There are several aspects of the coupled oscillator model that can be further developed as well as additional topics that can be studied using CFD:

- The frequency prediction of the coupled oscillator model should be improved. Finite element modeling could be used to inform the stiffness values in the coupled oscillator model.

- Presently, the model has only been applied to the first axial mode and needs to be validated for higher modes.

- The amplitude predictions from the model are quite conservative. Refinements to reduce this conservatism may be sought.

- CFD time histories could be applied as forcing to the coupled oscillator model to capture the effects of multi frequency excitation and phasing of the forces.

- It is suspected that higher-order fluid modes may exist for bellows as is the case for flow over rectangular cavities. This could be studied by conducting further bellows CFD simulations.

- There are several potential topics that could be studied further using CFD simulation. A CFD simulation of an angled bellows could help inform the affect this has on the bellows FIV characteristics. In addition, many bellows contain flow liners that significantly alter the flow characteristics in a bellows, but have been shown in literature to still be susceptible to FIV. If the forcing coefficients for partially lined convolutes can be found using CFD simulations, then they could be used with the coupled oscillator model to predict its FIV response. Another concept that could be studied using CFD is the flow field associated with variable pitch bellows. It is hypothesized that by having cavities of varying pitch, the bellow would not be able to strongly resonate since adjacent cavities would have different frequencies of fluid oscillations.

Bibliography

[1] K Sato. Flow induced vibration studies for LMFBR in Japan: Past and recent studies of FIV for JOYO and MONJU. Technical report, International Working Group on Fast Reactors, International Atomic Energy Agency, 1977.

[2] T Winkel and J Orchard. Leak evaluation in jet and its consequences for future fusion machines. *Vacuum*, 41(7-9):1988–1991, 1990.

[3] JES Venart. Flixborough: the explosion and its aftermath. *Process Safety and Environmental Protection*, 82(2):105–127, 2004.

[4] D Harland. *NASA's Moon Program: Paving the Way for Apollo 11*. Springer Science & Business Media, 2010.

[5] PJ Tygielski, HM Smyly, and CR Gerlach. Bellows flow-induced vibrations. Technical Report TM-82556, NASA Marshall Space Flight Center, Hunstville, AL, 1983.

[6] C Becht. *Behavior of bellows*. PhD thesis, Memorial University of Newfoundland, 2000.

[7] WF Anderson. Analysis of stresses in bellows. Technical report, North American Aviation. Atomics International Division., 1964.

[8] Expansion Joint Manufacturers Association. *Standards of the Expansion Joint Manufacturers Association*. Expansion Joint Manufacturers Association, 2008.

[9] F Salzmann. Uber die nachgeibigkeit von wellrohr-expansionen. *Schweiz, Bauztg*, 127(11):127–130, 1946.

[10] TM Trainer, LE Hulbert, JF Lestingi, RE Keith, et al. Final report on the development of analytical techniques for bellows and diaphragm design. *AFRPL Report No. TR*, pages 68–22, 1968.

[11] VR Daniels. Dynamic aspects of metal bellows. *The Shock and Vibration Bulletin*, (35 Part 3):107–124, 1966.

[12] CR Gerlach. Flow-induced vibrations of metal bellows. *Journal of Manufacturing Science and Engineering*, 91(4):1196–1202, 1969.

[13] CR Gerlach and EC Schroeder. Study of minimum pressure loss in high velocity duct systems. Technical Report NAS8-21133, Southwest Research Institute, 1969.

[14] CR Gerlach. Vortex excitation of metal bellows. *Journal of Manufacturing Science and Engineering*, 94(1):87–94, 1972.

[15] RL Bass and JL Holster. Bellows vibration with internal cryogenic fluid flows. *Journal of Manufacturing Science and Engineering*, 94(1):70–75, 1972.

[16] JE Johnson, DM Deffenbaugh, WJ Astleford, and CR Gerlach. Bellows flow-induced vibrations. Technical report, Southwest Research Institute, 1979.

[17] VF Jakubauskas. *Transverse Vibrations of Bellows Expansion Joints*. PhD thesis, McMaster University, 1995.

[18] AD Lytle. Dynamics of bellows filled with an incompressible liquid. *Journal of Spacecraft and Rockets*, 5(1):9–13, 1968.

[19] M Morishita, N Ikahata, and S Kitamura. Simplified dynamic analysis methods for metallic bellows expansion joints. *Journal of pressure vessel technology*, 113(4):504–510, 1991.

[20] TX Li, BL Guo, and TX Li. Natural frequencies of U-shaped bellows. *International Journal of Pressure Vessels and Piping*, 42(1):61–74, 1990.

[21] M Radhakrishna and CK Rao. Axial vibrations of U-shaped bellows with elastically restrained end conditions. *Thin-walled structures*, 42(3):415–426, 2004.

[22] VF Jakubauskas and DS Weaver. Axial vibrations of fluid-filled bellows expansion joints. *Journal of pressure vessel technology*, 118(4):484–490, 1996.

[23] VF Jakubauskas and DS Weaver. Transverse vibrations of bellows expansion joints. part II: beam model development and experimental verification. *Journal of Fluids and Structures*, 12(4):457–473, 1998.

[24] VF Jakubauskas and DS Weaver. Transverse natural frequencies and flow-induced vibrations of double bellows expansion joints. *Journal of fluids and structures*, 13(4):461–479, 1999.

[25] GI Broman, AP Jönsson, and MP Hermann. Determining dynamic characteristics of bellows by manipulated beam finite elements of commercial software. *International Journal of Pressure Vessels and Piping*, 77(8):445–453, 2000.

[26] CK Rao and M Radhakrishna. Transverse vibrations of double bellows expansion joint restrained against rotation. In *10th International Conference on Nuclear Engineering*, pages 499–506. American Society of Mechanical Engineers, 2002.

[27] M Radhakrishna and CK Rao. Vibration of double bellows type expansion joint in lateral and rocking modes. *International Journal of Structural Stability and Dynamics*, 6(04):575–588, 2006.

[28] CK Rao and M Radhakrishna. Dynamics of multiply expansion bellows with elastically restrained ends. In *ASME 2005 International Mechanical Engineering Congress and Exposition*, pages 69–76. American Society of Mechanical Engineers, 2005.

[29] M Watanabe, N Kobayashi, and Y Wada. Dynamic stability of flexible bellows subjected to periodic internal fluid pressure excitation. *Journal of Pressure Vessel Technology*, 126(2):188–193, 2004.

[30] VF Jakubauskas. Added fluid mass for bellows expansion joints in axial vibrations. *Journal of pressure vessel technology*, 121(2):216–219, 1999.

[31] VF Jakubauskas and DS Weaver. Transverse vibrations of bellows expansion joints. part I: fluid added mass. *Journal of Fluids and Structures*, 12(4):445–456, 1998.

[32] PV Desai and L Thornhill. Fatigue behavior of flexhoses and bellows due to flow-induced vibrations. Technical Report NASA-CR-176481, Georgia Inst. of Tech., 1986.

[33] DS Weaver. On flow induced vibrations in hydraulic structures and their alleviation. *Canadian Journal of Civil Engineering*, 3(1):126–137, 1976.

[34] E Naudascher and D Rockwell. *Flow-Induced Vibrations: An Engineering Guide*. Dover Publications, 2005.

[35] RD Blevins. *Flow-induced vibration*. New York, NY (USA); Van Nostrand Reinhold Co., Inc., 1990.

[36] T Nakamura, S Kaneko, F Inada, M Kato, K Ishihara, T Nishihara, and NW Mureithi. *Flow-induced vibrations: Classifications and lessons from practical experiences*. Butterworth-Heinemann, 2013.

[37] CR Gerlach, RL Bass, JL Holster, and EC Schroeder. Bellows flow-induced vibrations and pressure loss. *Final Report, NAS8-21133 (5th edn), Southwest Research Institute, San Antonio, TX*, April 1973.

[38] CR Gerlach, RL Bass, JL Holster, and EC Schroeder. Flow-induced vibrations of bellows with internal cryogenic fluid flows. Technical report, Interim Technical Report, 1970.

[39] D Rockwell and E Naudascher. Review–self-sustaining oscillations of flow past cavities. *Journal of Fluids Engineering*, 100(2):152–165, 1978.

[40] DS Weaver and P Ainsworth. Flow-induced vibrations in bellows. *Journal of Pressure Vessel Technology*, 111(4):402–406, 1989.

[41] A Gidi and DS Weaver. A model study of flow induced bellows vibration. In *Proceedings of 6th International Conference on Flow Induced Vibration*, pages 497–503, 1995.

[42] A Gidi. An experimental study of flow induced bellows vibrations. Master's thesis, McMaster University, 1993.

[43] D Rockwell. Predction of oscillation frequencies for instable flow past cavities. *Transactions of the ASME. Journal of Fluids Engineering*, 99(12):249–299, 1977.

[44] G Baylac, J Planchard, JP Gregoire, and C Pailly. Calculation of acoustical resonances in irregular cavities with application to noise-induced stress in expansion joints. *Journal of Engineering for Industry*, 127(11):101–108, 1976.

[45] M Popescu, W Shyy, and ST Johansen. A model for flow-induced acoustics in corrugated pipes. In *47th AIAA Aerospace Sciences Meeting including The New Horizons Forum and Aerospace Exposition*, page 1417, 2009.

[46] M Popescu, ST Johansen, and W Shyy. Flow-induced acoustics in corrugated pipes. *Communications in Computational Physics*, 10(01):120–139, 2011.

[47] M Popescu. Behavior of flow-induced vibration in corrugated pipes. In *20th AIAA Computational Fluid Dynamics Conference*, page 3395, 2011.

[48] C Becht IV. Predicting bellows response by numerical and theoretical methods. *Journal of pressure vessel technology*, 108:335, 1986.

[49] F Osweiller. Design of an expansion joint by a finite element program – comparison with the EJMA standards. 168:87–94, 1989.

[50] D Mackenzie and JT Boyle. Development of a flexible bellows element for piping analysis. 168:67–72, 1989.

[51] TX Li, BL Guo, TX Li, and QC Wang. Stresses and fatigue failure of U-shaped bellows. 168:13–19, 1989.

[52] WP Schonberg, PA Beasley, GR Guinn, and AJ Bean. Static testing of U-shaped formed metal bellows. *International Journal of Pressure Vessels and Piping*, 41(2):207–226, 1990.

[53] C Becht IV. Fatigue of bellows, a new design approach. *International journal of pressure vessels and piping*, 77(13):843–850, 2000.

[54] YZ Zhu, HF Wang, and ZF Sang. The effect of environmental medium on fatigue life for U-shaped bellows expansion joints. *International journal of fatigue*, 28(1):28–32, 2006.

[55] S Stelmar. Cyclic fatigue in metal bellows. In *ASME 2013 Pressure Vessels and Piping Conference*. American Society of Mechanical Engineers, 2013.

[56] TX Li, TX Li, and BL Guo. Research on axial and lateral natural frequencies of bellows with different end conditions. In *International Symposium*, volume 86, 1986.

[57] D Rockwell and E Naudascher. Self-sustained oscillations of impinging free shear layers. *Annual Review of Fluid Mechanics*, 11(1):67–94, 1979.

[58] ML Facchinetti, E de Langre, and F Biolley. Coupling of structure and wake oscillators in vortex-induced vibrations. *Journal of Fluids and structures*, 19(2):123–140, 2004.

[59] G Birkhoff and EH Zarantonello. Jets, wakes, and cavities. *New York*, pages 294–295, 1957.

[60] RED Bishop and AY Hassan. The lift and drag forces on a circular cylinder oscillating in a flowing fluid. In *Proceedings of the Royal Society of London A: Mathematical, Physical and Engineering Sciences*, volume 277, pages 51–75. The Royal Society, 1964.

[61] RT Hartlen and IG Currie. Lift-oscillator model of vortex-induced vibration. *Journal of the Engineering Mechanics Division*, 96(5):577–591, 1970.

[62] RA Skop and OM Griffin. A model for the vortex-excited resonant response of bluff cylinders. *Journal of Sound and Vibration*, 27(2):225–233, 1973.

[63] WH Xu, YX Wu, XH Zeng, XF Zhong, and JX Yu. A new wake oscillator model for predicting vortex induced vibration of a circular cylinder. *Journal of Hydrodynamics, Ser. B*, 22(3):381–386, 2010.

[64] A Farshidianfar and H Zanganeh. A modified wake oscillator model for vortex-induced vibration of circular cylinders for a wide range of mass-damping ratio. *Journal of Fluids and Structures*, 26(3):430–441, 2010.

[65] RD Gabbai and H Benaroya. An overview of modeling and experiments of vortex-induced vibration of circular cylinders. *Journal of Sound and Vibration*, 282(3):575–616, 2005.

[66] AH Nayfeh. *Introduction to perturbation techniques*. John Wiley & Sons, 1993.

[67] F Menter. Zonal two equation $k-\omega$ turbulence models for aerodynamic flows. In *23rd fluid dynamics, plasmadynamics, and lasers conference*, 1993.

[68] M Gharib and A Roshko. The effect of flow oscillations on cavity drag. *Journal of Fluid Mechanics*, 177:501–530, 1987.

[69] SF Hoerner. Fluid dynamic drag. *Bricktown, NJ: Published by the author*, 1965.

[70] E de Langre. Frequency lock-in is caused by coupled-mode flutter. *Journal of Fluids and Structures*, 22(6):783–791, 2006.